

Department of Physics and Astronomy

University of Heidelberg

Diploma thesis
in Physics

submitted by

Thomas Nikodem

born in Paderborn, Germany

November 2011

Study of the Performance of a
Same-Side-Kaon-Tagging Algorithm for the
LHCb Experiment using $D_s^+ \rightarrow \phi\pi^+$ and
 $B_s^0 \rightarrow D_s^- \pi^+$ decays

This diploma thesis has been carried out by Thomas Nikodem
at the
Physikalisches Institut
under the supervision of
Prof. Dr. Stephanie Hansmann-Menzemer

Studie über die Leistung des Same-Side-Kaon-Tagging Algorithmus für den LHCb-Detektor an $D_s^+ \rightarrow \phi\pi^+$ und $B_s^0 \rightarrow D_s^- \pi^+$ Zerfällen:

Der Large Hadron Collider (LHC) ist ein Hochenergie Teilchenbeschleuniger. Obwohl er nur mit der Hälfte der geplanten Schwerpunktsenergie ($\sqrt{s} = 7$ TeV) läuft, haben bei diesen Energien schwere B Mesonen bereits einen großen Wirkungsquerschnitt. Am LHCb Experiment werden diese B Mesonen zeitabhängig analysiert, wobei die Quark-Zusammensetzung der B Mesonen bei ihrer Entstehung mit sogenannten Flavour Taggern wie den Same Side Kaon Tagger (SSKT) bestimmt wird. Die Leistungsfähigkeit der Flavour Tagger kann mit der Tagging Power angegeben werden, welche in dieser Studie an $D_s^+ \rightarrow \phi\pi^+$ und $B_s^0 \rightarrow D_s^- \pi^+$ Zerfällen für den SSKT gemessen worden ist. Bei beiden Zerfällen ist die erwartete Tagging Power durch eine Simulation deutlich besser als die an Daten gemessene, weshalb Größen die einen Einfluss auf den SSKT haben, wie Teilchenidentifikation oder Detektorauflösung, untersucht und wenn nötig in der Simulation angepasst werden. Es wird gezeigt, dass eine Korrektur in der Simulation von dem Underlying Event und der D_s^+ und B_s^0 Fragmentation die beobachteten Unterschiede in der Tagging Power erklären kann.

Study of the Performance of a Same-Side-Kaon-Tagging Algorithm for the LHCb experiment using $D_s^+ \rightarrow \phi\pi^+$ and $B_s^0 \rightarrow D_s^- \pi^+$ decays:

The Large Hadron Collider LHC is a high-energy particle accelerator. Running still at half the design energy the LHC provides proton proton collisions with a center of mass energy of $\sqrt{s} = 7$ TeV. This deduces a large cross section of heavy B mesons which are studied in the LHCb experiment time dependently. For time dependent studies the quark content of the B mesons at production time must be determined which is accomplished by flavour taggers like the Same Side Kaon Tagger (SSKT). The performance of flavour taggers can be expressed by the so called tagging power. The tagging power of the SSKT is studied using $D_s^+ \rightarrow \phi\pi^+$ and $B_s^0 \rightarrow D_s^- \pi^+$ decays. For both decays it is measured that the expected tagging power in simulation is significantly better as in data. Several properties related to tagging like particle identification or detector resolution are investigated and differences are corrected in simulation. The impact of each correction on the tagging power is measured. It is found that a possible explanation for the observed discrepancy in the tagging power between data and simulation would be a incorrect description of the underlying event and the D_s^+ and B_s^0 fragmentation.

Contents

1	Introduction	6
2	The LHCb Experiment	8
2.1	The Large Hadron Collider	8
2.2	The LHCb Detector	10
2.2.1	Tracking	11
2.2.2	Particle Identification	12
2.2.3	Trigger	15
2.3	Physics Program	16
3	Event Simulation	18
3.1	Event Simulation at LHCb	18
3.2	Event Generation in Pythia	18
3.2.1	The Event	18
3.2.2	Fragmentation	20
4	Flavour Tagging at LHCb	23
4.1	Same Side Tagger	24
4.2	Opposite Side Taggers	29
4.3	Quality variables	31
5	Performance of the Same Side Kaon Tagger for D_s^+ mesons	32
5.1	D_s^+ Selection	33
5.2	Default Tagging Performance	35
5.3	Data and Simulation Comparison	36
5.3.1	Trigger	36
5.3.2	Primary Vertex Multiplicity	39
5.3.3	Track Resolution	40
5.3.4	Particle Identification	42
5.3.5	Underlying Event	46
5.3.6	Fragmentation	50
5.4	Summary	55
6	Performance of the Same Side Kaon Tagger for B_s^0 mesons	56
6.1	B_s^0 Selection	57
6.2	Default Tagging Performance	60
6.3	Data and Simulation Comparison	63
6.3.1	Primary Vertex multiplicity	63
6.3.2	Track Resolution	63
6.3.3	Particle Identification	64
6.3.4	Underlying Event	66
6.3.5	Fragmentation	69
6.4	Summary	72

7	Summary and Conclusion	74
A	Optimizing D_s^+ Same Side Kaon Tagger	76
B	Estimating the mistag probability for the mixing B_s^0 meson	78

1 Introduction

One of the greatest achievements of the last century was the observation of symmetry breaking. For a long time it has been presumed as a fact that physics was the same, independent of space, time or charge. Only in 1956, Chien-Shiung Wu discovered parity breaking of the weak interaction in the decay of Co-60 atoms, therefore falsifying this statement [1]. This means that in a universe reflected on a point in comparison to ours, indeed, physics would be different.

After this discovery it was assumed that instead physics was invariant for both the charge (C) and parity (P) transformation applied together. This CP symmetry is preserved in the experiment of Wu. Furthermore, redefining matter as antimatter and vice versa after this transformation would allow physics to be described the same. However, in 1964 J. Cronin, V. Fitch et. al. showed in the decay of heavy neutral K mesons that this CP symmetry is broken as well [2].

Meanwhile CP violation is explained by the so called Standard Model of particle physics, a theory which describes all elementary particles and their interactions. Although all effects observed in laboratory experiments are well explained by this model, it is e.g. not able to explain the large excess of matter in the universe. Thus there must be additional sources of CP violation which would be physics beyond the Standard Model, so called new physics.

The B system is an excellent place to study CP violation as due to loop suppression of tree level contributions in B decays new physics is expected to have large interference effects. However, there are many different B decay modes and thus each mode has a small branching ratio. Thus to do precision measurements large statistics is needed. This is given for example at high-energy accelerators like the Large Hadron Collider (LHC) [3] which have a large B cross section. At the LHC two protons collide at a center of mass energy of $\sqrt{s} = 7$ TeV and therefore, along with Tevatron [4], LHC provides today the unique possibility to study large samples of B hadrons such as B_s^0 . From the four detectors at the LHC, it is LHCb which is dedicated to explore B-physics. LHCb is a forward arm spectrometer with a good track reconstruction, vertex resolution and particle identification, offering the right conditions to do time-dependent analyses of B hadrons.

An important property of the B_s^0 meson is its oscillation. Due to weak processes the B_s^0 is able to transform into a \bar{B}_s^0 . Therefore the flavour content of the B_s^0 is not a conserved quantity but changes over time. For time dependent analyses the flavour content of the B_s^0 must be measured at different times. At decay time this can be done by reconstructing the decay products. In contrast it is more complex to measure the production flavour of a B hadron. Several correlations of the B hadron to other particles cre-

ated alongside in the collision are exploited in so called flavour taggers to determine the original flavour content and *tag* this information on the reconstructed B hadron. For the B_s^0 one of these flavour taggers is the Same Side Kaon Tagger (SSKT), analyzed in this diploma thesis.

In the proton collision, due to flavour conservation in the strong interaction, with the B_s^0 always a particle containing an anti-strange quark is created. This other particle is correlated to the production flavour content of the B_s^0 and is tried to identify with the SSKT algorithm. Due to this correlation the SSKT only works for one of the B hadrons, the B_s^0 , and thus the algorithm can only be calibrated on its data samples. Because of the fast B_s^0 mixing frequency large statistics is required. An alternative would be to tune the SSKT algorithm on simulation. Therefore it would be crucial to have an agreement between data and simulation with regard to detector simulation and also the description of the B_s^0 fragmentation process. The detector simulation can be checked as well in the similar D_s^+ system.

In the D_s^+ system there is not only large statistics available due to a high cross section but also because of its charge the D_s^+ does not oscillate. Therefore its flavour content at production time is the same as at decay time. Using this information the tag of the SSKT can be checked directly. Therefore, the D_s^+ system is ideal to analyze the SSKT algorithm and also the simulation.

In this diploma thesis the SSKT performance is studied on data and on simulation. In chapter 2 an overview of the LHCb experiment is given. The production of simulated data used in this study is presented in chapter 3. Afterwards the different flavour tagging algorithms applied in LHCb are introduced in chapter 4. The SSKT is studied and compared to simulation first on D_s^+ decays in chapter 5 and then on the B_s^0 decays in chapter 6. Finally, in chapter 7 the observed results are discussed.

2 The LHCb Experiment

The LHCb is one of the experiments of the European Organization for Nuclear Research CERN [5] located in Meyrin near Geneva. CERN is an international organization which was founded in 1954. It consists today of 20 European member states.

It is involved in pure research of particle physics and besides other discoveries the one of neutral currents can be attributed to CERN. At the moment its main contribution to research in physics is the operation of the Large Hadron Collider (LHC). In the LHC protons are accelerated to high energies in the TeV scale providing high cross sections also for heavy particles.

Four experiments are located at the LHC. Studies about quark-gluon plasma are done by the ALICE experiment (A Large Ion Collider Experiment). The ATLAS experiment (A Toroidal LHC Apparatus) is searching for heavy particles, for example the Higgs boson, and new physical models like SUSY. CMS (Compact Muon Solenoid) is also a multipurpose detector searching for new physics.

LHCb is dedicated to B-physics. Precision measurements of the standard model and measurements of CP violation with B mesons are done. At the moment the B_s^0 meson is marginally studied and new results are expected to be obtained.

In section 2.1 the LHC will be presented. Afterwards in section 2.2 the LHCb detector will be explained. At the end in section 2.3 the physics program of LHCb is outlined.

2.1 The Large Hadron Collider

The LHC is a particle accelerator located near Geneva (see figure 1). It is placed in a 27 km long circuit tunnel up to 175 m below the earth's surface of the Swiss-Franco border.

The LHC is a typically synchrotron with two parallel beam pipes in which protons are accelerated in opposite directions. At the location of the experiments the beam pipes cross and there are particle interactions. To keep the protons on the circuit track there are superconducting magnets which provide B fields up to 8.3 T.

The proton beams are not constant, they are split up into several bunches of about 10^{11} protons each. The time between two bunches in one beam is designed to be 25 ns, so proton proton interactions appear with 40 MHz. With this settings it will be possible to produce a luminosity up to 10^{34} $\text{cm}^{-2} \text{s}^{-1}$.

The design energy of these proton beams is 7 TeV per proton. This would result in a center of mass energy at the interaction of $\sqrt{s} = 14$ TeV. At the moment the LHC is operating at half of this energy which means a center of mass energy at the interaction point of $\sqrt{s} = 7$ TeV.

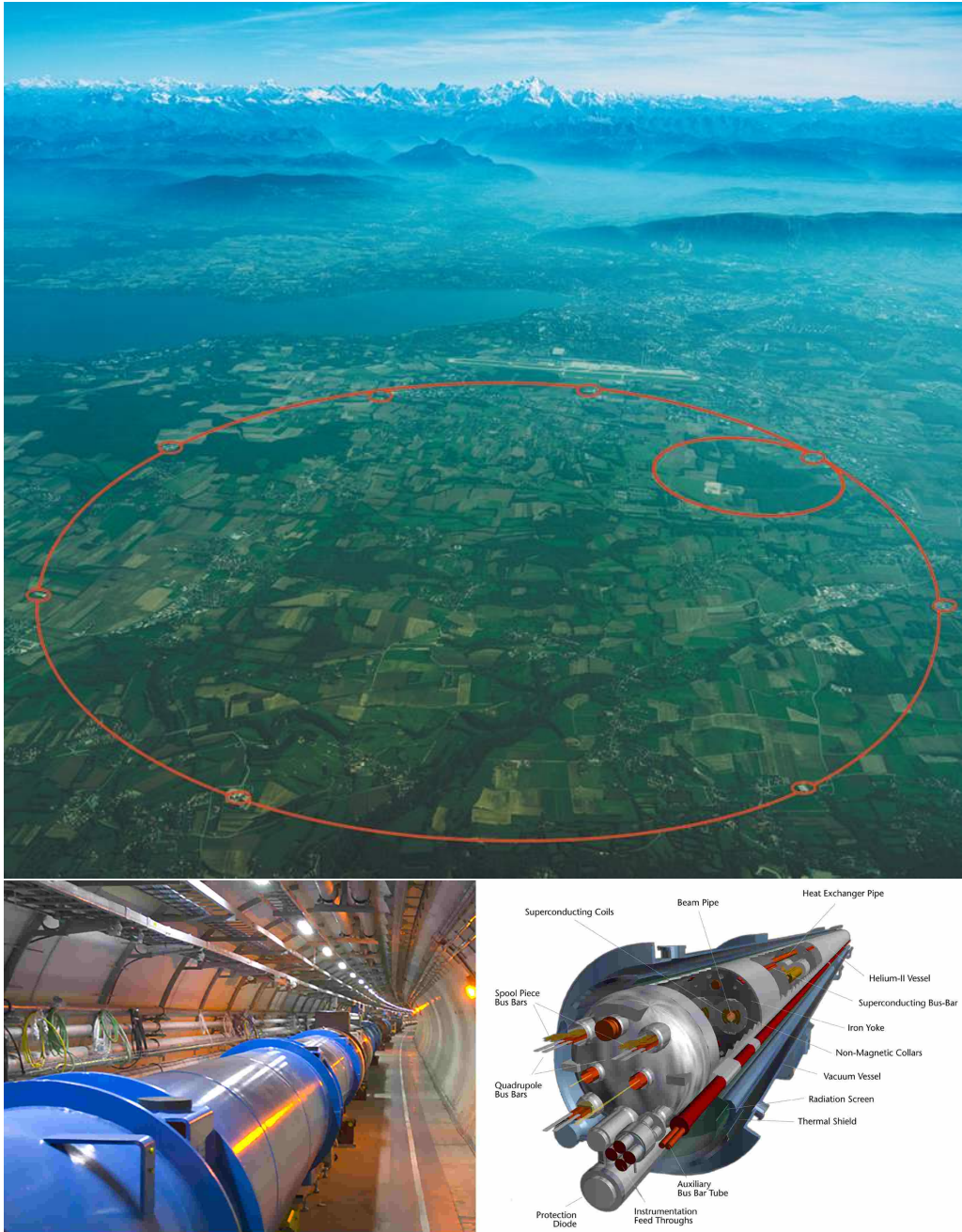


Figure 1: Top: The location of the 27km long tunnel of the Large Hadron Collider (LHC) near Geneva. Bottom: photo of the tunnel (left) and structure of the beam pipe (right). The LHC is today the world most powerful particle collider. It accelerates protons to a center of mass energy at collision of $\sqrt{s}=7$ TeV. With this high energy there is also a large cross section of heavy mesons like the B_s^0 . [7]

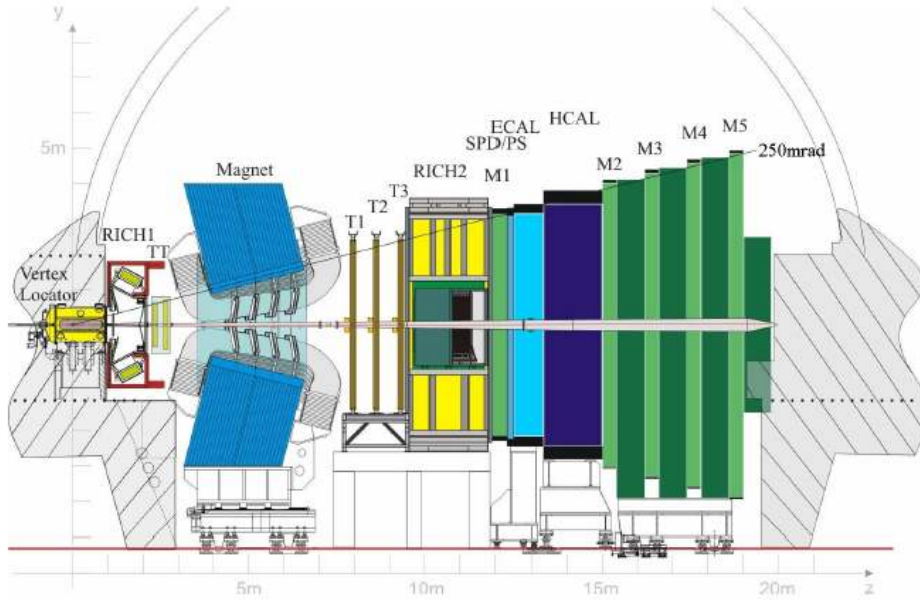


Figure 2: Side view of the LHCb Detector[6]. The different sub detectors are highlighted in different colors. The heavy B mesons are busted in forward and backward directions and thus most of them can be detected within the 250 mrad coverage of the LHCb detector.

Besides from protons also lead atoms will accelerated to an energy of 574 TeV per nucleus.

2.2 The LHCb Detector

In the high energetic interactions the heavy quarks are produced dominantly in the high eta regions near the beam pipe, therefore for studying B mesons there is no need for a 4π detector. Due to this reasons the LHCb detector is a forward arm spectrometer (see figure 2) covering the pseudorapidity region from $1.6 < \eta < 4.9$.

The coordinate system of LHCb is a right handed one, in which the z axis corresponds to the beam pipe and the y axis is showing upwards. The zero point is the place of the proton proton interactions.

To measure precisely the primary vertex and also further decay vertices of short living particles the VERTex LOcator (VELO) is built. Behind the VELO the RICH1 detector is attached to separate protons, kaons, pions and electrons. For the particle identification there is also the RICH2 detector located behind the magnet and the tracking stations.

The particle momentum is measured with a magnetic field of 4 Tm along the z axis. This is achieved by a saddle shaped dipole magnet. The track reconstruction of charged particles is done with the Trigger Tracker (TT) before the magnet and the Inner Tracker (IT) and Outer Tracker (OT) after the magnet. Uncharged photons and neutral pions are detected in an

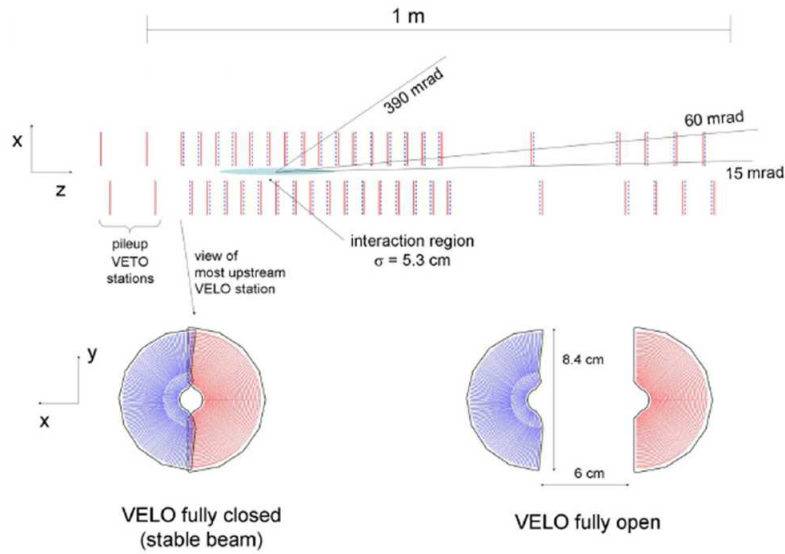


Figure 3: The VERtEX LOcator (VELO) of the LHCb detector[6]. It consists out of 46 silicon modules which can be moved up to a distance of 5 mm to the interaction region.

electronic calorimeter (ECAL) and hadronic calorimeter (HCAL). At the end of the detector there are five muon chambers separated each with 80cm of iron to identify muons.

2.2.1 Tracking

The direction and the magnitude of the momentum of particles is measured by several detectors in combination with the magnet. The charged particles move in a circular orbit due to the magnetic field. The radius of this orbit is proportional to the momentum of the particle. Therefore reconstructing the track of a particle the magnitude and also the originally direction of the momentum can be determined. Tracks are reconstructed in the VELO, the TT as well as in the T-stations (T1-T3). With combining the track parts of all of these sub detectors to one track one receives the so called Long Tracks. The Long Tracks are the default track type in physics analyses.

The VELO (see. figure 3) is a silicon detector and is located where the heavy D and B mesons are created. The VELO is movable as it is located closer to the interaction region as it is the width of the proton beam during initialization at LHC. When stable proton beam is declared the two VELO halves are closed and the inner radius of the detector is only 8 mm from the center of the beam. With using the VELO a primary vertex resolution of about 13 μm in x/y direction and 70 μm in z direction is obtained which results in a proper time resolution of B mesons of about 45 fs.

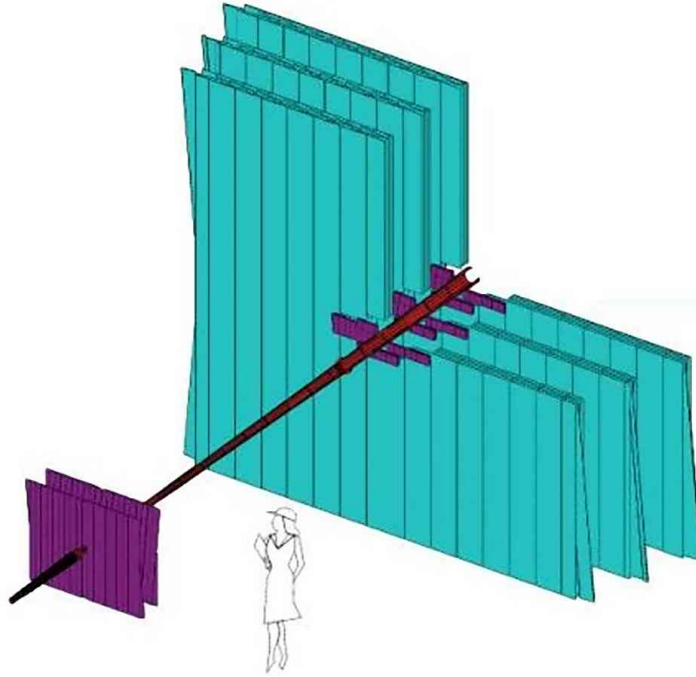


Figure 4: The Inner Tracker (purple) and Outer Tracker (turquoise). While the IT is a silicon detector the OT consists out of straw tubes and is a drift chamber. For better resolution layers of each station are rotated by 5° to each other.[6].

The Inner Tracker (IT), which consists of the TT and the inner part of the T-stations (see. figure 4), is also a silicon detector. The IT is a rectangular detector which is split up to vertical stripes of a width of $70\ \mu\text{m}$. Each station of the TT has two layers which are rotated 5° to each other to also provide resolution into the vertical direction. The largest uncertainty of the track reconstruction in this detector is coming from multiple scattering of the particles. Because of this the detectors are built with as few material as possible.

The outer part of the T stations (OT) as shown in figure 4 is made of straw tubes filled with a gas mixture of $\text{Ar}:\text{CO}_2:\text{O}_2 = 70:28.5:1.5$. In the middle of each tube is an anode wire and thus each detector is a drift chamber. An OT station is build out of four layers which are like the TT also rotated by 5° with respect to each other. The OT provides access to a large η range while providing a sufficient spacial resolution of about $220\ \mu\text{m}$.

2.2.2 Particle Identification

For B mesons decaying in pions and kaons it is important to distinguish these particles at reconstruction. This is done with two Ring Imaging CHerenkov (RICH) detectors. RICH1 is placed upstream the VELO directly in front of the TT. RICH2 is placed after the T stations in front of the calorimeters. The two detectors differ in angular acceptance regions and the optimal mo-

momentum region for the detected particles. Whereas RICH1 is built for low momentum particles for the full angular detector acceptance RICH2 is especially designed to identify high momentum particles. These particles are not bend by the magnetic field very strong and thus are still near the beam pipe.

The principle of RICH detectors uses the Cherenkov light. Compared to sound cones of supersonic jets also particles have light cones if they are moving faster than the light speed of the medium. The emitted photons have a specific angle:

$$\cos\theta = \frac{1}{n\beta}$$

where n is the refractive index and $\beta = v_p/c$ is the ratio of the speed of the particle to the speed of light in vacuum. Thus the angle θ only depends on the speed of the particle. Different angles are expected in the RICH detectors (see figure 5).

The light cone shows on a image plane a ring with a velocity specific radius. The momentum of a particle is known due to the the curvature of the track inside the magnetic field. Identifying and combining the ring and the track is one of the major challenges of the RICH software. However knowing both the momentum and the Cherenkov angle the mass of a particle can be determined.

Both RICH detectors are shown in figure 6. RICH1 has a polar acceptance of 25-300 mrad horizontally and 25-250 mrad vertically, thus all particles reconstructed in tracking can theoretically also be identified. Its momentum range is from 1-60 GeV. The used media is for the very slow particles aerogel and for the faster ones C_4F_{10} gas. To reduce the material budget in the particle flux the Cherenkov light is reflected with mirrors to the sides of the detector. There positioned high density photo multipliers record these photons. The photo multipliers are shielded with metal to exclude background radiation and also be able to operate in the strong magnetic field.

RICH2 covers only a polar acceptance of 12-120 mrad horizontally and 12-100 mrad vertically. It is designed for particles with 15 GeV up to above 100 GeV and therefore the used medium is CF_4 gas. Like in RICH2 the Cherenkov photons are reflected by mirrors to the outside.

The provided information from the RICH systems is a measure of the probability that a particle is of one kind with respect to another kind. This is done via the Delta Log Likelihood (DLL) of two particle hypothesis. For example it is

$$DLL_{k\pi} = (\ln\mathcal{L}(K) - \ln\mathcal{L}(\pi)) = \ln\frac{\mathcal{L}(k)}{\mathcal{L}(\pi)}$$

where \mathcal{L} is the likelihood of the particle hypothesis.

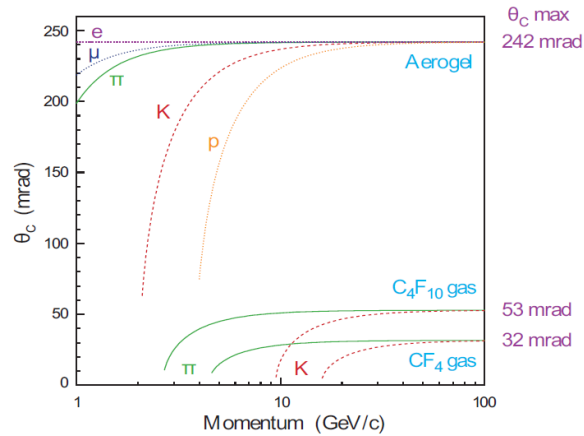


Figure 5: The Cherenkov angles of different particles for media used in RICH1 (Aerogel and C_4F_{10}) and RICH2(CF_4) [6]. With RICH detectors protons p, kaons K, pions π and electrons e are distinguished from each other.

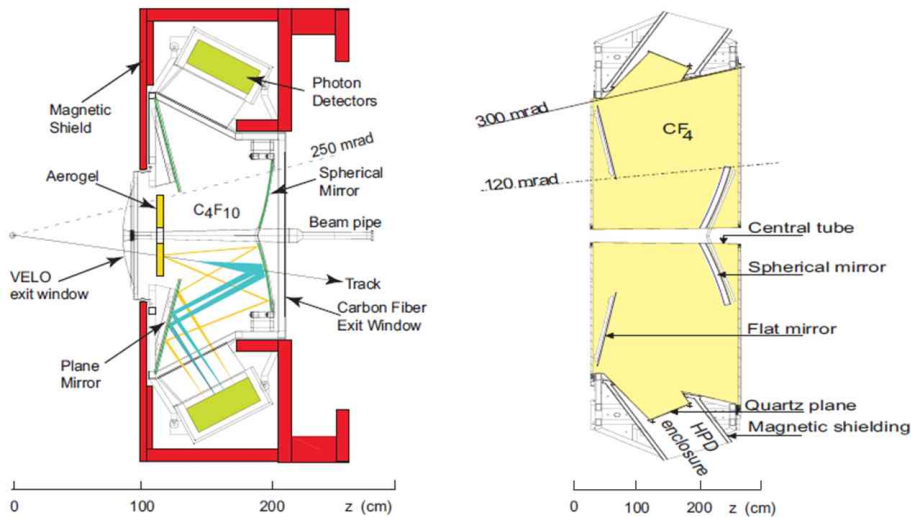


Figure 6: Both Ring Imaging Cherenkov (RICH) detectors used in LHCb for particle identification [6]. RICH1 (left) works for the full angular detector acceptance whereas RICH2 (right) is especially build for high momentum particles only little distracted by the magnet and thus are still near the beam pipe.

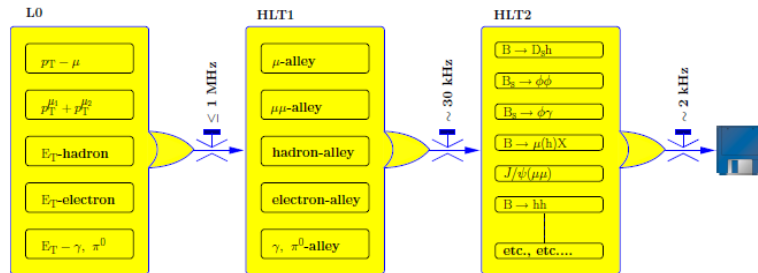


Figure 7: The three trigger stages(L0, HLT1, HLT2) in the LHCb experiment[6]. With every trigger stage more specific event details are required and thus despite of the original bunch crossing rate of 40 MHz, events are written on tape with only at 2 kHz.

2.2.3 Trigger

The proton proton collisions are produced in LHCb with a frequency of about 40 MHz. However saving all information from every event would be too much data to handle. Only events at a rate of about 2 kHz can be written on tape. This requires a good selection on the fly of the important events which should be saved for later analyses. Therefore a trigger system is implemented in LHCb which reconstructs particles online. The trigger is subdivided into three stages, first Level0(L0) and then High Level Trigger HLT1 and HLT2 (see figure 7).

The L0 is build out of electronics and synchronized to the bunch crossing of the LHC. The main detectors used in the L0 are the calorimeters and for particle decays into muons the muon stations. The calorimeters are typical sampling calorimeters with different width for electrons and hadrons. With them it is triggered on events with a particles with high transverse energy and on events with a high total transverse energy in general. In front of the calorimeters with a Scintillator Pad Detector (SPD) the track multiplicity in the event can be estimated. Events with too many tracks and too much combinatorial possibilities are rejected. Altogether the rate is reduced from 40 MHz to 1 MHz.

In contrast to L0 the HLT triggers are software based and thus can be adjusted. The triggers run on a server farm and have in principle access to all data of the event and can do everything what is also done in the later physics analysis.

The HLT itself is subdivided into the HLT1 and the HLT2. Due to time pressure no full event reconstruction can be done. The event is only analyzed partly. The main task of HLT1 is the reconstruction of charged tracks in the VELO and T-stations. A high transverse momentum of the particle and a good track quality are required. Furthermore uncharged tracks, measured in the calorimeters, are confirmed with the absence of a track in the T-

stations. This is the so called L0 confirmation. In the HLT1 the event rate is further reduced to about 30 kHz.

This rate is low enough to do a full event reconstruction in the HLT2. For analyses specific trigger decisions can be set. For example for an analysis on the $B_s^0 \rightarrow D_s^- \pi^+$ decay the presence of a ϕ meson in the event can be required. With HLT2 the rate is reduced to acceptable 2 kHz.

2.3 Physics Program

The main physics program of the LHCb experiment is measuring B mesons. Predictions of theory, the Standard Model of particle physics, can be compared to the measurements. Possible differences can be assigned to additional contributions from undiscovered particles. These additional contributions would be physics beyond the Standard Model, so called new physics. Searching indirectly for effects of new particles is complementary to the direct search of them done by ATLAS and CMS. Due to loop suppression of tree level contributions in the B-system it is for these B mesons where new physics is expected to have large interference effects.

There are two approaches at LHCb to check Standard Model predictions. First is checking Flavour Changing Neutral Current (FCNC) decays, for example $B_s^0 \rightarrow \mu^- \mu^+$, which are supposed to have small branching ratios. It is expected that new physics might have a large effect on these branching ratios.

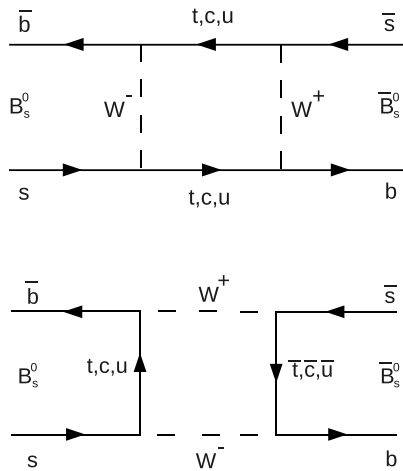


Figure 8: Dominating Feynman diagrams responsible for B_s^0 mixing.

Second is measuring CP violation in for example the mixing of neutral B mesons (B^0 and B_s^0). Uncharged B mesons (and D^0 , K^0) can spontaneously transform into their antiparticles and vice versa. This is described in the weak interaction with the help of the Cabibbo–Kobayashi–Maskawa (CKM) matrix. The according Feynman diagrams can be seen in figure 8. As the

number of quarks is conserved in the Standard Model the CKM matrix is unitary. Checking this unitarity allows to excluding or finding new physics. To measure mixing of B mesons their quark content must be measured time dependently. At decay time the quark content can be reconstructed via the decay products. The reconstruction of the flavour content of the B mesons at production time is done with so called flavour taggers (see chapter 4) like the same side kaon tagger. They are a crucial part of these analyses. Detailed information about the LHCb physics program can be found in [8] and [9].

3 Event Simulation

3.1 Event Simulation at LHCb

For many physics analyses at the LHCb experiment there is the need to rely on simulated data. Firstly, this simulated data is used if there is not enough statistics of data available. For example, in rare decays the particle selection algorithm can be tuned based on the simulation. The expected number of background events can be estimated with the simulation and compared to the measurement. This is especially important if only a small number of particles (<10) is expected to be measured.

Secondly, with the simulation issues can be investigated which would not be possible on data. For example the detector acceptance can be measured by looking how many generated particles would be detected. The precise knowledge of the detector acceptance is important especially for cross section measurements.

Thirdly there is the possibility to access so called MC truth information. The true identity of reconstructed particles is saved and can be used to test and calibrate different algorithms. For example it can be checked if the proposed tagging decision from the flavour taggers (see chapter 4) is correct and an expectation of the quality of the algorithm can be given.

Event generation at LHCb is done in two steps. In the first step with the knowledge about different particle cross sections an event is generated. This is done by GAUSS [10]. GAUSS itself uses, among others, PYTHIA [11] for the event generation and EvtGen [12] for simulating decays of B mesons. With this event information BOOLE [13] simulates afterwards the detector response.

Especially the event generation is an important part for flavour taggers as the correlations of the production of particles in the proton proton collision are exploited in the algorithms. For this reason there will be a closer look at Pythia in the next section.

3.2 Event Generation in Pythia

The physical models presented in this section are implemented in Pythia. The following refers to the Pythia Manual [14] and a lecture given by its author T. Sjostrand [15].

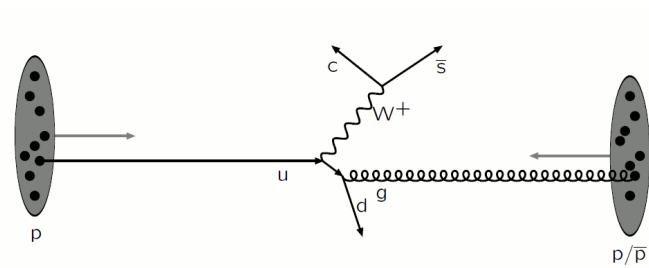
3.2.1 The Event

As can be seen in figure 9 the event generation is split in several steps. Assuming to be in the LHC environment at the beginning there are two incoming protons. These protons consist of dynamic quarks and gluons.

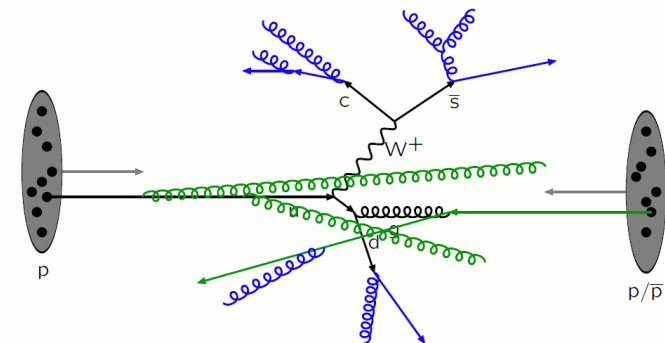
a) Colliding Hadrons



b) The Hard Subprocess



c) Initial(green) and Final(blue) State Radiation



d) Multiple Parton-Parton Interaction with its Initial and Final State Radiation

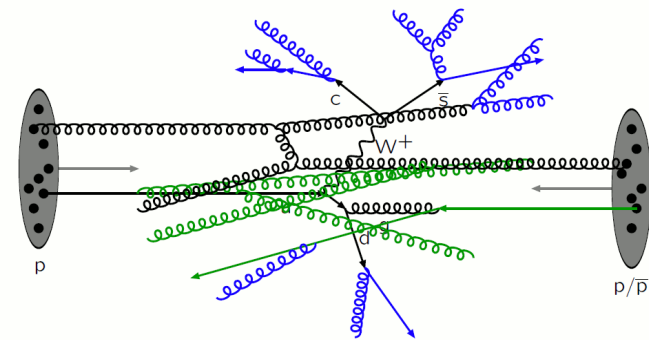


Figure 9: The Generation of an event in Pythia [15]. Different models are implemented for the different processes.

The probability for finding specific quarks with specific momenta is given by the Parton Density Function [16] and is simulated accordingly.

In the next step two out of these partons are interacting in hard processes and produce e.g. a W-Boson and a quark jet as shown in figure 9b. This process is perturbatively calculable and with matrix elements the cross sections can be determined. Many of these produced particles, like the W-Boson, are unstable and decay immediately. These decays are correlated with the collision and still can be calculated perturbatively in a similar way.

However additionally there is the much more complex final- and initial state radiation (see figure 9c). In a simple way this can be thought of in the same way as electrical charge is radiating photons, color charge is emitting gluons. This can no longer be expressed with matrix elements but must be handled with the parton shower model.

Furthermore the other partons in the protons are not immobile but there is also multiple parton-parton interaction occurring which again has final and initial state radiation (see figure 9d).

After producing quarks and gluons the fragmentation takes place. Due to the linear potential in the strong interaction the gluons and quarks are confined. This is simulated by connecting them with an object called a string. When the quarks are propagating away from each other and the string tension gets large enough it breaks up. With the field energy new particles are created which form color neutral hadrons that do not couple to the color field.

The majority of these hadrons is however not stable and decays in different leptons and (more) stable hadrons. These remaining particles are finally the ones which are measured in the detectors.

3.2.2 Fragmentation

Because this is important for flavour tagging (see chapter 4) one should have a closer look at the fragmentation. This is implemented in Pythia with the LUND string model.

As described above when the energy in the string between two quarks is large enough a new quark pair with the appropriate colors can be created out of the vacuum. In a classical picture this process can be described by creating 2 virtual particles tunneling in energetically allowed regions.

It follows that in the center of mass system of two quarks the probability for creating a new quark pair is proportional to [14]

$$P(m_{\perp}^2) \propto \exp\left(-\frac{\pi m_{\perp}^2}{\kappa}\right) = \exp\left(-\frac{\pi m^2}{\kappa}\right) \exp\left(-\frac{\pi p_x^2}{\kappa}\right) \exp\left(-\frac{\pi p_y^2}{\kappa}\right),$$

where the original quarks are flying along the z-direction, $m_{\perp} = \sqrt{E^2 - p_z^2}$ is the common transverse mass of the new quarks and $\kappa \approx 1 \text{ GeV/fm}$ is the string tension.

With higher quark masses the probability for the production decreases drastically. The relative probabilities for the different quarks are u:d:s:c = 1:1:0.3:10⁻¹¹. Therefore no heavy quarks are expected to be created in the fragmentation. The probability of creating $s\bar{s}$ quark pairs is a tuning parameter as this model is purely phenomenological and not expected to be valid in all physics scenarios.

The exponential function can be split up and thus the fragmentation can be handled independently for different quark masses and for the two dimensions. In a good approximation the transverse momentum distributions are Gaussian and it is their root mean square to which MC is tuned. Nevertheless the distributions have non-Gaussian components which can lead to problems [14].

Having set the transverse momenta still the longitudinal momenta of the new quarks must be determined. This is however constrained by the transverse mass m_{\perp} .

One possible choice is to regard the hadron to be created out of the original quark and one of the new quarks. Then the free parameter is z , the fraction of $E + p_z$ (Energy plus the longitudinal momentum) of the original quark taken by the hadron. A fragmentation function $f(z)$ gives the probability that a certain z value is chosen.

In history many different fragmentation functions were tested for agreement. The default function is the LUND SYMMETRIC FRAGMENTATION FUNCTION [14](p. 366):

$$f(z) \propto \frac{1}{z} z^{a_{\alpha}} \left(\frac{1-z}{z} \right)^{a_{\beta}} \exp\left(-\frac{bm_{\perp}^2}{z}\right)$$

where a_{α} , a_{β} and b are tuning parameters.

For heavy quarks a different approach, the PETERSON FRAGMENTATION FUNCTION [17], gives the best results. From the standard quantum-mechanical parton-model follows that the transition amplitude is proportional to the inverse of the energy difference. Because heavy quarks are only influenced slightly by light quarks the invariant mass of the system should stay the same. Thus the energy difference between the two states, before (heavy quark m_Q) and afterwards (meson $m_H \approx m_Q$ and light quark m_q), is expected to be:

$$\Delta E = (m_Q^2 + z^2 P^2)^{1/2} + (m_q^2 + (1-z)^2 P^2)^{1/2} - (m_Q^2 + P^2)^{1/2}$$

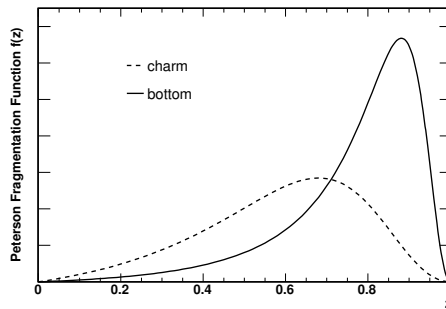


Figure 10: Peterson Fragmentation Function[17] for charm and bottom quarks. The probability of keeping more of the over all momentum is for bottom quarks than for charm quarks.

From this can be concluded that for high momentum P it is:

$$f(z) \sim \frac{1}{z[1 - (1/z) - \epsilon_Q/(1-z)]^2}$$

where the tuning parameter $\epsilon_Q \sim \frac{m_q^2}{m_Q^2}$ is proportional to the effective quark mass ratio squared.

As for the bottom quark ϵ_Q is about a factor 10 smaller than for a charm quark, the bottom quark keeps in the mean a much higher part of the momentum (see figure 10). Therefore there is less momentum for the other particles created in the Fragmentation, which are interesting for the Tagger. Even if the lower momentum ratio is compensated with the overall higher momentum in the B-system, the shape still stays different.

The fragmentation process is described in Pythia by a phenomenological model with two main tuning parameters. On the one hand there is the transverse mass distribution and on the other hand there is the fragmentation function. These parameters were tuned on data from LEP and Tevatron [18] and extrapolated to the higher energies used at LHC ($\sqrt{s} = 1$ TeV at Tevatron compared to $\sqrt{s} = 1$ TeV at LHC).

The fragmentation itself is expected to be different for charm and bottom quarks. Because in the B-system the light quark is more negligible and the overall momentum is higher the assumptions in the Peterson Fragmentation are more valid for bottom than for charm quarks. This is especially the case if, like in the Same Side Kaon Tagger (see section 4.1), the light quark is not an up or down but a strange quark.

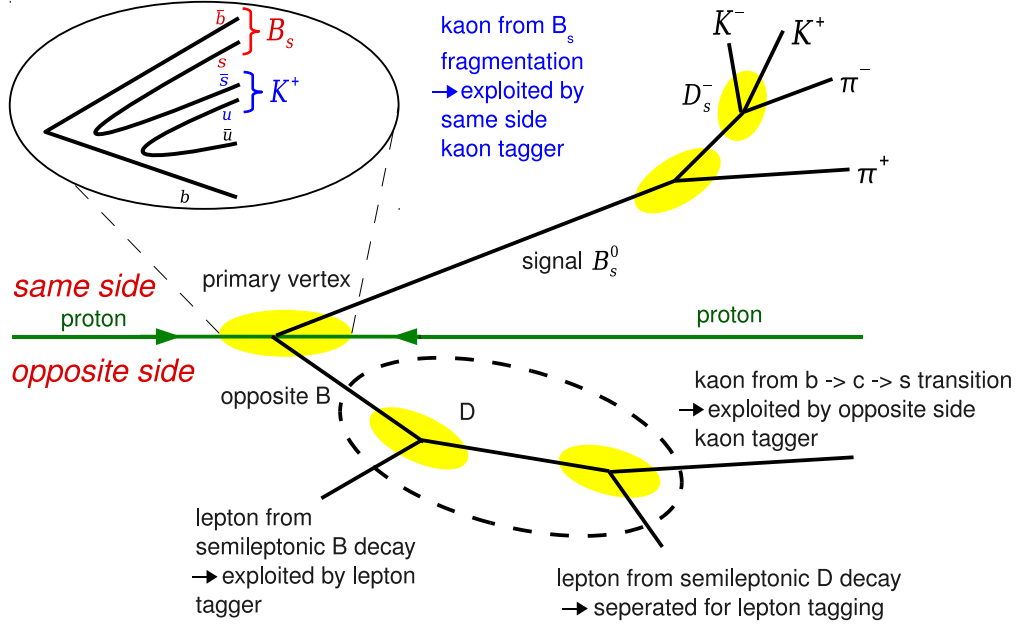


Figure 11: Schematic of the physical processes used by the Flavour Tagging algorithm[24].

4 Flavour Tagging at LHCb

As already pointed out in section 2.3 it is important to have reliable information about the production flavour of B mesons. The physical processes involved in tagging are sketched in figure 11. There are two different approaches which are included in the tagging algorithm.

The so called opposite side taggers exploit the fact that in strong interactions bottom quarks are produced in flavour conjugated pairs. Thus, there are two B hadrons in the event which have the opposite bottom quark flavour. Several decay products of the B hadrons are specific for their flavour content at decay time. Thus if certain particles are present in the event the flavour of the other B hadron can be determined. With the assumption that the other B hadron did not oscillate the original signal B_s^0 flavour can be concluded.

The other approach is the same side tagging. Analogously to the bottom quarks also the strange quarks are produced in flavour conjugated pairs. Thus with the strange quark of the signal B_s^0 also an anti-strange quark is created. This forms a hadron which determines the quark content of the signal B_s^0 . Identifying this hadron is the task of the same side tagger.

Whereas in the opposite side taggers particles with a large Impact Parameter (IP, see figure 14) are selected, in the same side taggers particles with small impact parameters coming directly from the Primary Vertex (PV) are used. Therefore both algorithms are orthogonal in phase space and can be applied independently from each other. Only at the very end their results are combined into one tagging decision.

B_s^0 Fragmentation

Created Quarks			Associated Particles			Probability
(b) \bar{b}	s	\bar{s}	u (\bar{u})	B_s^0 K^+ π^0	18.9%	
			d (\bar{d})	B_s^0 K^+ π^-	18.9%	
			s (\bar{s})	B_s^0 K^+ K^-	5.7%	
		d	\bar{d}	u (\bar{u})	B_s^0 K^0 π^+	18.9%
				d (\bar{d})	B_s^0 K^0 π^0	18.9%
				s (\bar{s})	B_s^0 K^0 \bar{K}^0	5.7%
	s	\bar{s}	u (\bar{u})	B_s^0 ϕ K^+	5.7%	
			d (\bar{d})	B_s^0 ϕ K^0	5.7%	
			s (\bar{s})	B_s^0 ϕ ϕ	1.7%	

Table 1: Left column: Subset of possible quarks created in the B_s^0 fragmentation. Middle column: Particles that can be created out of these quark combinations. Only the lightest particle states are considered. Right column: The probability that these particles are created. The quark production probability is $u\bar{u}:d\bar{d}:s\bar{s} = 1:1:0.3$ (see section 3.2.2). In about 50% of the cases (bold) with a B_s^0 also a K^+ is created. This correlation is used in the SSKT.

In the following there is a further description of the same side tagger in section 4.1 and the opposite side tagger in section 4.2. In section 4.3 the figures of merit, the tagging efficiency, the mistag probability and the tagging power are explained.

4.1 Same Side Tagger

The same side tagger depends on the signal B meson. Therefore there is the same side pion tagger which is used for B^0 mesons and the Same Side Kaon Tagger (SSKT) which is constructed for the B_s^0 mesons. In the following only the SSKT will be presented.

The SSKT exploits the fact that in many cases with the B_s^0 also a K^+ is created in the fragmentation. Due to flavour conservation in the strong interaction along with the $B_s^0(\bar{b}s)$ there is always a \bar{s} quark produced. According to the models used in Pythia (see section 3.2.2) this is combined in

43.5% of the cases with an up quark, in 43.5% with a down quark and in about 13% with another strange quark.

This fragmentation process is visualized in table 1. In the left column the created quark pairs in the several fragmentation steps are listed. For the B_s^0 creation in the first step a $b\bar{b}$ quark pair and then a $s\bar{s}$ quark pair are created. For the next fragmentation step there are the three possibilities: up, down or strange quark pair. At every step these three choices are possible. For reasons of complexity only the first four fragmentation steps are listed. Quarks produced even further down in the fragmentation process are uncorrelated to the B_s^0 and would deliver no useful information with respect to tagging.

Out of these quark combinations a manifold set of particles is created, which can be seen in the middle column. In the table only the lightest particle states are listed, as heavier particles decay afterwards in these ground states (e.g. BR: $K^*(892) \rightarrow K^+\pi^- = \sim 100\%$, decay width: 50.8 ± 0.9 MeV [19]). The probabilities for each of these particle combinations are shown in the very right column. What can be seen is that in 50% of the cases a K^+ is (directly) formed. However also negative K^- are created directly or as decay products from ϕ mesons (BR $\phi(1020) \rightarrow K^+K^- = 48.9 \pm 0.5\%$ [19]). The SSKT algorithm tries to identify the K^+ . As seen above this is only created in about half of the cases and for the other cases there is no correlation to exploit. Therefore the SSKT can at maximum give half of the B_s^0 the right tag.

The tagging is accomplished by the SSKT in the following way. All charged tracks in the event are considered¹. Then by cutting on several (kinematic) track quantities, PID variables and other useful observables most of the background tracks are dismissed. If after these cuts there is no track left no tag is given by the tagger. If there is however more than one track passing all cuts the one with the highest transverse momentum gives a tagging decision according to its charge. A $K^+(u\bar{s})$ deduces that the meson was a $B_s^0(\bar{b}s)$ at production time and vice versa.

Several background sources are polluting the SSKT. There are ghosts which are tracks created in the track reconstruction and not originating from real particles. The χ^2 of the track fit is then however predominately larger than normal and thus they can be separated. Also tracks from different PVs wrongly associated to the signal PV are contributing to the background. However, their distance to the signal PV is mostly much larger than for the kaons of interest and they have predominantly a large IP.

Nevertheless there is also background which consists of real particles coming from the signal PV. On the one hand there is the so called Underlying Event (UE). These are tracks created in the collision of two protons but which are not correlated to the signal B.

¹Only a subset of tracks which are clearly uninteresting (Signal B_s^0 decay products, tracks from different PVs, everything besides Long Tracks) is ignored in the first place.

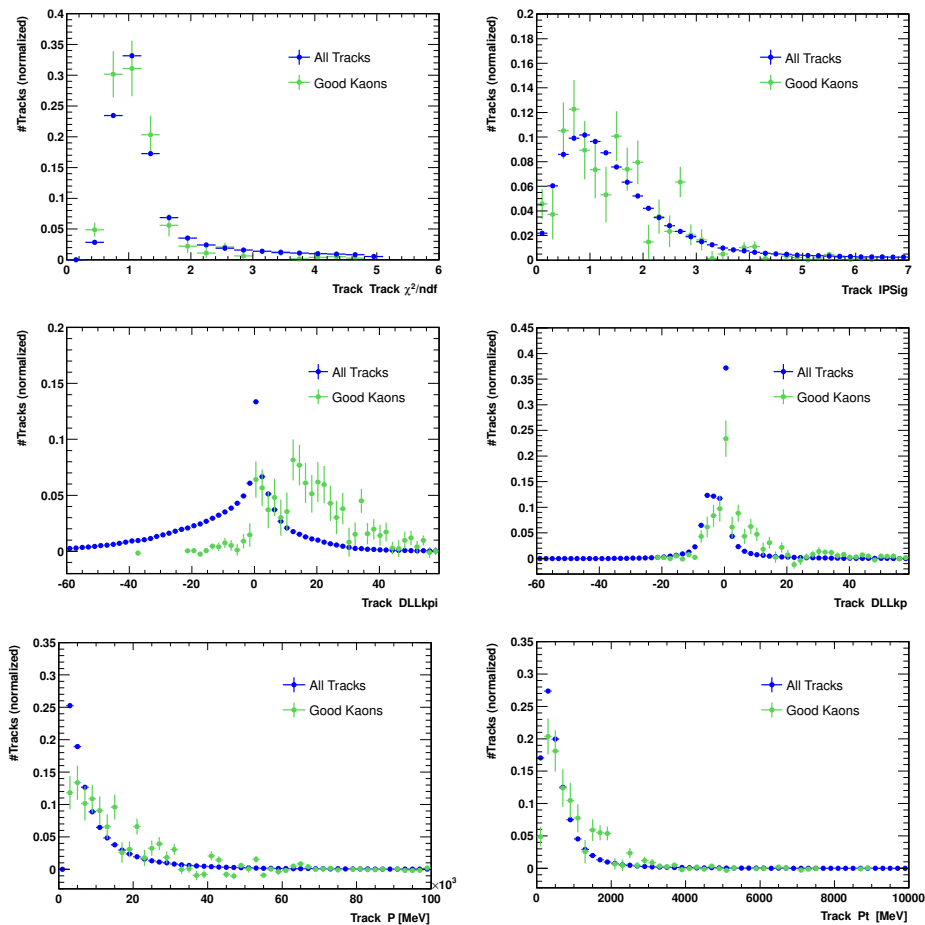


Figure 12: Distribution of variables which are used in the SSKT algorithm to separate the *good kaon* from the B_s^0 fragmentation. All tracks in the event with a loose preselection (blue) are compared to the kaons from the B_s^0 fragmentation which would give the right tagging decision (green).

On the other hand there are, as seen in table 1, also kaons created directly in the signal fragmentation which would give the wrong tag. Their properties are identical to the ones with the right charge.

The major contribution to the background after the selection cuts listed below comes from the UE. It is responsible for 76% of the tracks which would give the wrong tagging decision. About 19% of these tracks are from the B_s^0 fragmentation, 4% of the tracks are related to the opposite side decay. Only 5% of the tracks originate from other sources, such as ghosts².

To handle the background there are several quantities available which can be used to separate it. They are shown in figure 12 and figure 13 for all tracks in the event with a loose preselection (see table 14 in section 6.1)

²According to the B_s^0 MC simulation presented in section 6.

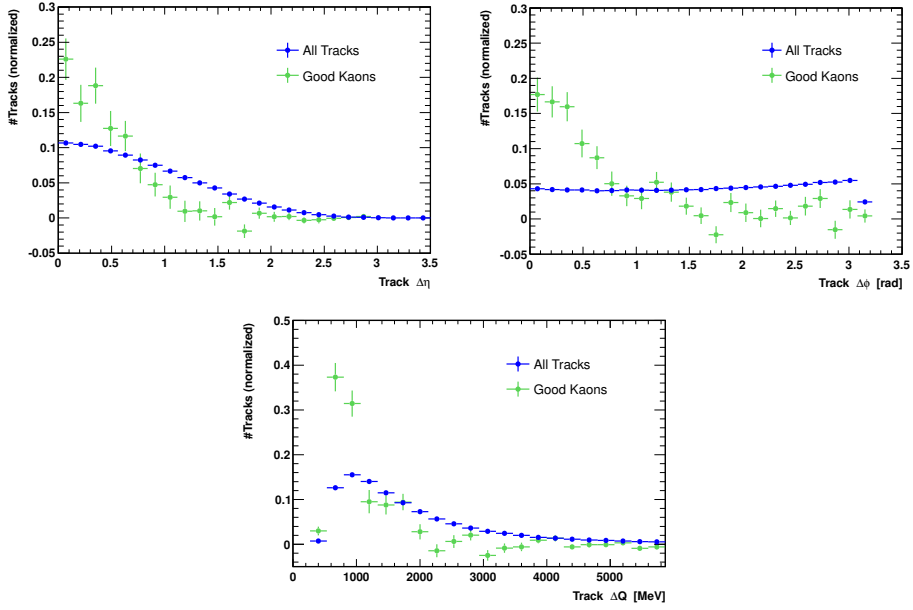


Figure 13: More quantities used in the SSKT algorithm. The B_s^0 fragmentation tracks are mainly located close to the B_s^0 meson in phase space.

and the good kaons³ from the B_s^0 fragmentation which the SSKT tries to identify. The quantities are:

- **Track χ^2/ndf (default cut: < 3.75)**

Track χ^2 divided by number of degree of freedoms represents the goodness of the track fit. Its value should be one. Most of the bad reconstructed tracks or ghosts are excluded by this cut.

- **IPSig (Impact Parameter Significance, default cut: < 4.125)**

The Impact Parameter (IP) is the distance from the PV to the track (see 14). Correspondingly the IPSig is the Impact Parameter divided by the IP uncertainty σ_{IP} given by the track fit.

$$IPSig = \frac{IP}{\sigma_{IP}}$$

Particles with a small IPSig were produced predominately directly in the PV. Compared to the IP this variable has a better separation power between particles coming from the PV and from displaced vertices.

³The *good kaons* were required to originate from the same string as the B_s^0 (see section 3.2.2). Furthermore all kaons with the wrong charge compared to the tagging decision are subtracted from the ones with the right charge. The remaining kaons are the ones the SSKT tries to identify.

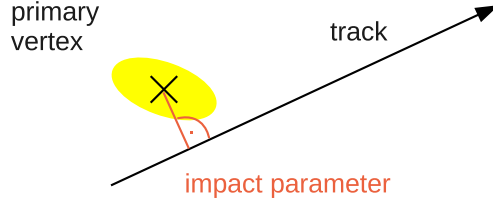


Figure 14: Sketch of the Impact Parameter (IP) used in the SSKT. The IP is the distance from a track to the primary vertex.

- Particle Identification (default cuts: $DLL_{kpi} > 4.5$, $DLL_{kp} > -8.5$)**
 These variables distinguish kaons from pions and protons respectively. The DLL is the combined output from the particle identification detectors discussed in section 2.2.2.
- Momentum(P) and Transverse Momentum(Pt)(default cuts: $P > 5250$ MeV, $Pt > 750$ MeV)**
 These variables have a good separation power between signal and background. Mesons containing bottom quarks are produced with higher energy in comparison to the other particles. The tagging kaon comes from the same center of mass system and thus it is also high-energetic. In the SSKT dominantly the transverse momentum is used as it is more significant than the momentum.
- $\Delta\eta = |\eta_{track} - \eta_B|$ (see figure 15, default cut $\Delta\eta < 0.525$)**
 The pseudorapidity η is defined as

$$\eta = -\ln \left[\tan \left(\frac{\theta}{2} \right) \right]$$

where θ is the angle of the momentum vector of the particle with respect to the beam pipe. The kaon from the B_s^0 fragmentation is supposed to be near in phase space to the signal B_s^0 and thus $\Delta\eta$ should be small.

- $\Delta\phi = |\phi_{track} - \phi_B|$ (see figure 15, default cut $\Delta\phi < 0.7$ rad)**
 In the xy plane orthogonal to the beam pipe, ϕ is the angle between the momentum vector of the particle and the x axis⁴. The difference in ϕ of the kaon to the B should be small.

⁴For a definition of the coordinate system see section 2.2

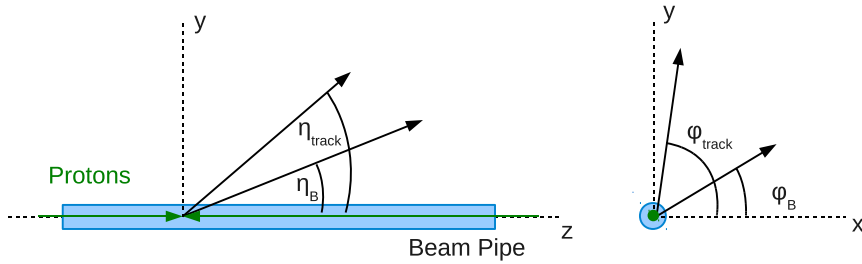


Figure 15: The variables $\Delta\eta = |\eta_{track} - \eta_B|$ (left) and $\Delta\phi = |\phi_{track} - \phi_B|$ (right) used in the SSKT. If the kaon is related to the B_s^0 both particles fly dominantly in a similar same direction.

- ΔQ ($\text{mass}(B_s^0 + K^+) - \text{mass}(B_s^0)$, default cut: $\Delta Q < 1463$ MeV)
 ΔQ is another possibility to express the phase space relations. The probed track is assumed to be a kaon. The invariant mass of a hypothetical particle consisting out of the B and the track is calculated and compared to the B mass. As the right kaon shares the strange quark pair with the B there should be only little additional energy.

To reject ghosts and background from different PVs almost all cuts have a good rejection power. However it is hard to abandon background from the UE. This can be done with the $\Delta\eta$, $\Delta\phi$ and ΔQ variables. Nevertheless tracks from the UE may also be accidentally close in phase space to the B_s^0 and thus be mismatched as the right B_s^0 fragmentation track.

Also the Pt cut can separate the particles connected to the high energetic B_s^0 fragmentation from the rest. It is, however, hard to distinguish particles from the same fragmentation from each other. Only with the particle identification detecting pions also this background from the B_s^0 fragmentation can be identified.

4.2 Opposite Side Taggers

Because of the flavour conservation in the fragmentation process the bottom quarks are produced in pairs. One bottom quark forms the signal B_s^0 which is reconstructed. The other bottom quark forms any B hadron, called in the following opposite B .

Due to the bottom quark the opposite B decays weakly and hence it has a large lifetime. Thus, the decay products can be well distinguished from particles coming directly from the PV. This is used in the single particle taggers (electron, muon, kaon). Furthermore an inclusive reconstruction of the B is done in the vertex charge tagger.

Challenging for the opposite side tagger is the oscillation of the neutral opposite B mesons. In the algorithm it is assumed that the opposite B did not

change its flavour content before its decay. Therefore, this would result in a wrong tagging decision even if the B decay was correctly reconstructed. During their lifetime 19% of the B^0 transforms into their antiparticle. In contrast 50% of the fast oscillating B_s^0 change their flavour content before their decay. Thus the B_s^0 have no tagging information to exploit.

Electron/Muon Tagger

There are two main sources for leptons in the B decay. Either the lepton comes directly from the B (e.g. for both e^- , μ^- Branching Ratio $B^0 \rightarrow \ell^+ \nu_\ell$ anything: $10.33 \pm 0.28\%$ [19]) or indirectly from a decay product of the B (most often D).

Only the first contribution is interesting because of the direct link between the charge of the lepton and the flavour of the B . In the latter decay the leptons have dominantly the opposite charge and thus would result in a wrong tag.

To select only the interesting leptons a hard momentum cut is used. In the decay the original energy is distributed between the different decay products. Thus in longer decay chains the leptons are lower energetic and can be separated by kinematic variables. [23]

Kaon Tagger

The bottom quark usually decays into a charm quark which is transformed into a strange quark. In this decay chain a kaon is created. Its charge is associated to the flavour of the opposite B . To select kaons from B hadrons and not from the fragmentation the kaons are required to have large IPSig[24].

Similar to the Lepton Tagger there are as well other kaons coming from the B decay which would give the wrong tag. Compared to the kaon from the D these are however expected to be less energetic and thus rejected with additional momentum cuts.

Vertex Charge Tagger

Another strategy is not to look at single particles but to reconstruct inclusively the opposite B . Tracks are if possible assembled to a secondary vertex which is assumed to be at the place where the opposite B decayed. A weighted charge Q_{vtx} of the tracks from this vertex is calculated and according to this number a tagging decision is chosen. The track charge is weighted by the transverse momentum[24]:

$$Q_{\text{vtx}} = \frac{\sum_i p_T^\kappa(i) Q_i}{\sum_i p_T^\kappa(i)}$$

with κ a tuning parameter, Q_i the charge of the i^{th} track and $p_T(i)$ is its transverse momentum.

4.3 Quality variables

The power of a Flavour Tagger (FT) can be described by two quantities. The tagging efficiency

$$\epsilon = \frac{\text{all tagged signal } B \text{ mesons}}{\text{all signal } B \text{ mesons}}$$

describes in how many cases a decision can be made at all. The other variable is the mistag probability

$$\omega = \frac{\text{wrong tagged signal } B \text{ mesons}}{\text{all tagged signal } B \text{ mesons}}$$

A small ω means that the algorithms works well and only a few particles are identified incorrectly.

The FT is used in time dependent analyses like the B_s^0 mixing. The sensitivity (Signal/Noise) of such oscillation measurements is described by [20]:

$$\frac{S}{N} = \sqrt{\frac{\epsilon \cdot n}{2}} (1 - 2\omega) e^{-\frac{(\Delta m_s \cdot \sigma_{ct})^2}{2}}$$

Where n is the number of events, Δm_s is the oscillation frequency, σ_{ct} the proper time resolution and ϵ , ω are the quantities described above. The variables n and σ_{ct} are determined by the data selection efficiency and the detector. Concerning the FT the so called Tagging Power

$$q = \epsilon (1 - 2\omega)^2$$

must be maximized. This variable is the figure of merit for each FT.

At $e^- e^+$ colliders a typical Tagging Power is 28% (BaBar [21]). In the very clean events of lepton-antilepton colliders FT are working excellently. The usual Tagging Power at hadron colliders is only in the region of 5% (CDF [22]). Tagging is one of the main challenges of B-physics at hadron colliders.

5 Performance of the Same Side Kaon Tagger for D_s^+ mesons

Time dependent flavour studies in the B_s^0 system require good flavour taggers like the Same Side Kaon Tagger (SSKT) algorithm which was discussed in the last chapter. To achieve the best tagging performance the algorithms are optimized.

This optimization could be done on part of the B_s^0 sample, however this would reduce the statistics available for the physics analysis. Another possibility would be to tune on simulated events. However, this can only be done if the MC simulation can be trusted.

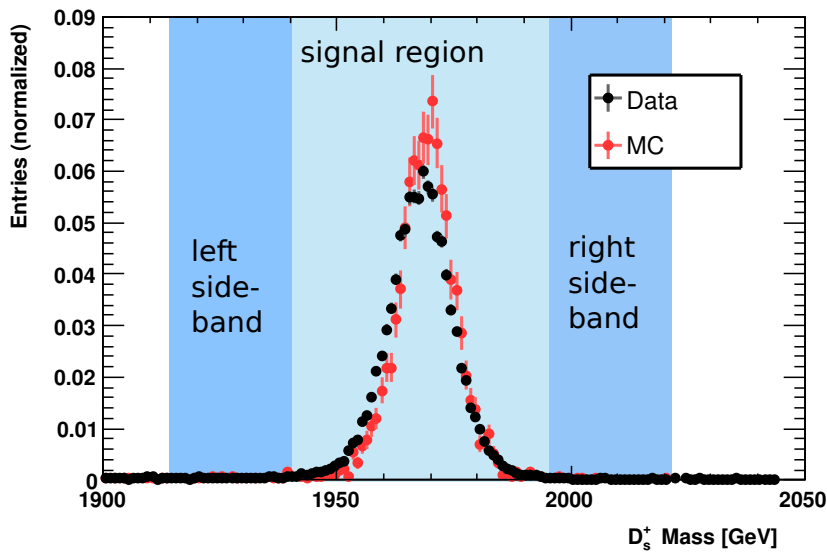


Figure 16: D_s^+ mass of data and MC simulation. The remaining background in the signal region will be corrected for with two sidebands.

A possibility to test the SSKT on data as well as testing the simulation for agreement is the D_s^+ system. The SSKT can only be used to probe mesons which contain a strange quark. Along with this strange quark in the fragmentation also an anti-strange quark is created which in 50% of the cases forms the kaon used in the SSKT algorithm⁵. The D_s^+ consists analogously to the B_s^0 of a strange quark and a heavy quark. For both physics can be described by the Peterson Fragmentation (see section 3.2.2) in which the fragmentation process is dominated by the heavy quark. Thus although the phase space of the fragmentation tracks in the D_s^+ and B_s^0 system may differ the physical processes are theoretically the same. Furthermore both the Underlying Event (UE) and the detector response are assumed to be independent of the fragmentation. Thus the SSKT algorithm can be tested and compared to the simulation in the D_s^+ system.

⁵A full description of the SSKT algorithm can be found in section 4.1

Analyzing the SSKT in the D_s^+ system brings about several advantages. Due to charge conservation the D_s^+ does not oscillate. Therefore its flavour content at decay time is the same as at production time. Thus for each D_s^+ the tagging decision of the SSKT can be checked with the reconstructed flavour content. This makes it possible to test the SSKT algorithm also on data. Finally another advantage is the large amount of D_s^+ data available which can be analyzed.

In this chapter MC simulation is compared to data. Quantities related to the tagging performance such as track multiplicity, particle identification variables and momentum distributions are studied. Potential differences of the detector simulation like a worse impact parameter resolution in data compared to MC simulation or a different PID performance are corrected for. The remaining discrepancy between data and MC simulation is compared to a possible not perfect description in the MC generation.

5.1 D_s^+ Selection

The data-set used in this analysis contains the first 36 pb^{-1} of LHC taken in 2010 at a center of mass energy of $\sqrt{s} = 7 \text{ TeV}$. A corresponding MC simulation is available which is analyzed in the same way as data.

To separate real D_s^+ from background several cuts to the data samples are made. The list of event selection cuts can be seen in table 2. To prevent correlation between two reconstructed D_s^+ only events with exactly one reconstructed D_s^+ per event are taken. Events with a too high track density are rejected by a cut on the maximum number of Primary Vertices (PV).

To be able to compare data and MC simulation this analysis is restricted to certain trigger requirements which will be presented in section 5.3.1.

A clean D_s^+ mass peak with low background is achieved with the D_s^+ selection cuts listed in table 3. Only D_s^+ which decay into $\phi (K^+ K^-) \pi^+$ are selected to exploit the ϕ resonance. The reconstructed ϕ mass must match the PDG[19] value within a range of 15 MeV. To reject low momentum background the D_s^+ momentum is required to be at least 2 GeV. The quality of the decay vertex reconstruction is checked with a vertex χ^2 cut. The decay particles of the D_s^+ are also required to have a minimum momentum of 2 GeV and transverse momentum of 250 MeV. The χ^2 of the track fit of the D_s^+ daughters divided by the number of degrees of freedom (Track χ^2/ndf) is selected to be smaller than 5. To suppress tracks which in reality come from the PV, D_s^+ daughters must have an $\text{IPSig} > 3$. Furthermore a minimum D_s^+ proper time is required. The separation of pions and kaons is done with the $\text{DLLkpi} > 2$ cut for kaons and $\text{DLLkpi} < -2$ cut for the pion.

The D_s^+ mass distribution can be seen in figure 16. Although combinatorial background is for the D_s^+ system only of the order of 2%⁶ these wrongly re-

⁶Expectation due to the amount of D_s^+ in the mass sidebands

Event Selection	
number of D_s^+	1
number of Primary Vertices	≤ 3

Table 2: Event selection for D_s^+ sample

D_s^+ Selection	
only $D_s^+ \rightarrow \phi(\rightarrow K^+K^-)\pi^+$ (and charge conjugated)	
ϕ Mass	1019.445 ± 15 MeV
Pt	> 2 GeV
proper lifetime ($c\tau$)	> 0.1 mm
Vertex χ^2	< 25
D_s^+ daughters	
Track χ^2	< 5
Pt	> 250 MeV
P	> 2 GeV
IPSig	> 3
DLLkpi	> 2 (kaons), < -2 (pions)

Table 3: Cuts to select D_s^+ signal candidates

constructed particles would reduce the measured tagging performance. To handle the background three mass regions are defined. Particles in a window of 4σ around the PDG D_s^+ mass (1940-1994 MeV) are weighted with 1. The regions 1913-1940 MeV and 1994-2021 MeV, together covering the same mass range as the signal region, are defined as sidebands. Particles with these masses receive the weight -1 in the plots and thus are subtracted. As the combinatorial background is assumed to be uncorrelated to the mass the background in the peak region should cover the same phase space. Therefore it should cancel by subtracting the appropriate number of background events. All the following results are sideband corrected.

With this selection the number of D_s^+ candidates is 2635 for MC simulation and 28598 for data.

Tagging Track Selection	
Track Type	Long Tracks
IPSig to D_s^+ PV	$<$ IPSig to any other PV
IPSig to any other PV	> 3
$\Delta\phi$ (track \leftrightarrow each D_s daughter)	> 0.015 rad
θ (track \leftrightarrow beam pipe)	> 0.012 rad

Table 4: Tagging Track selection used to select tracks potentially interesting for the SSKT. The following analysis will be based on this selection.

SSKT Cuts	
P	> 4000 MeV
Pt	> 850 MeV
IPSig	< 5
Track χ^2/ndf	< 5
$\Delta\eta$	< 0.8
$\Delta\phi$	< 0.9 rad
ΔQ	< 1600
DLLkpi	< 5
DLLkp	< -5

Table 5: Tuning of the SSKT algorithm used in this chapter to determine the tagging power. The cuts are optimized on MC simulation.

The SSKT uses tracks in the event to determine the production flavour of the D_s^+ . Only tracks potentially interesting for the SSKT will be investigated. They will be called in the following *Tagging Tracks*. Their selection is based on the preselection of the default SSKT[24] and is shown in table 4. Only tracks detected by all sub detectors, so called *Long Tracks*, are chosen. Their IPSig with respect to the D_s^+ PV is required to be smaller than to any other PV in the event. Furthermore they are not allowed to come too close to other PVs. In the track reconstruction track parts from the VELO and T-stations can be wrongly associated and also used twice. This would result in two reconstructed tracks with similar properties, so called clones. For the SSKT cloned Tagging Tracks would be not a problem, as the charge of the cloned track stays predominantly the same. Only clones of D_s^+ decay products would confuse the tagging algorithm. To rejected cloned D_s^+ decay products a Tagging Track is required to have a ϕ value which is different to each D_s^+ daughter in at least 0.015 rad. Finally tracks with a too small angle θ and therefore small distance to the beam pipe are excluded to prevent badly reconstructed tracks due to multiple scattering in the beam pipe.

The final cuts used in the SSKT algorithm to calculate the tagging decision are listed in 5. For the D_s^+ system these cuts were received by optimizing them on MC simulation. This optimization process will be discussed in appendix A.

5.2 Default Tagging Performance

With the selection presented in section 5.1 the SSKT performance is measured for data and MC simulation. The Tagging Power (see section 4.3) is determined by exploiting the fact that the D_s^+ is not oscillating. The tag given by the SSKT is compared to the flavour content of the D_s^+ decay products. In this way it is not only possible to determine the fraction of D_s^+ which are tagged, but also measure the fraction of D_s^+ which have the wrong

Tagging Performance

	Tagging Efficiency	Mistag Probability	Tagging Power
	ϵ	ω	$\epsilon(1 - 2\omega)^2$
Data	0.2163 ± 0.0024	0.3554 ± 0.0061	0.0181 ± 0.0015
MC	0.2296 ± 0.0082	0.2926 ± 0.0185	0.0395 ± 0.0072

Table 6: Tagging performance for the D_s^+ selection presented in section 5.1. There is a discrepancy in the mistag probability ω of 0.062 ± 0.020 .

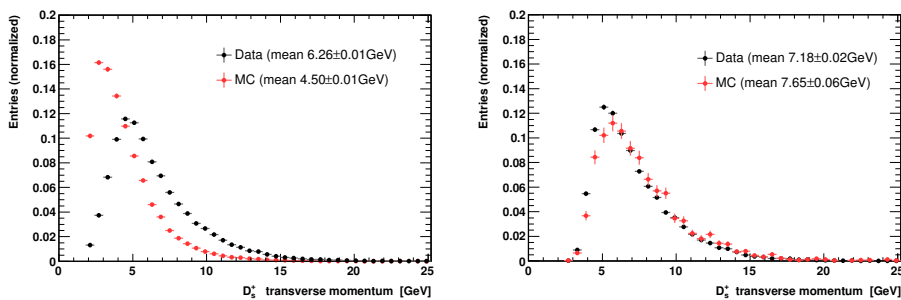


Figure 17: D_s^+ transverse momentum before(left) and after(right) trigger decision requirements

tag. With this information the tagging performances shown in table 6 are derived.

The Tagging Power in MC simulation is significantly larger than in data. That is why it is necessary to have a closer look at the simulation. The tagging efficiency ϵ seems to be consistent and the mistag probability ω seems to be the reason for the disagreement. The discrepancy in ω amounts 0.062 ± 0.020 .

Therefore quantities which are important for the SSKT algorithm like the track resolution or PID performance will be examined.

5.3 Data and Simulation Comparison

5.3.1 Trigger

On MC simulation the trigger has to be emulated to reject events that would not have passed the trigger during online data taking (triggering was explained in section 2.2.3). There are several different trigger decision subsets available to select the events important for this analysis.

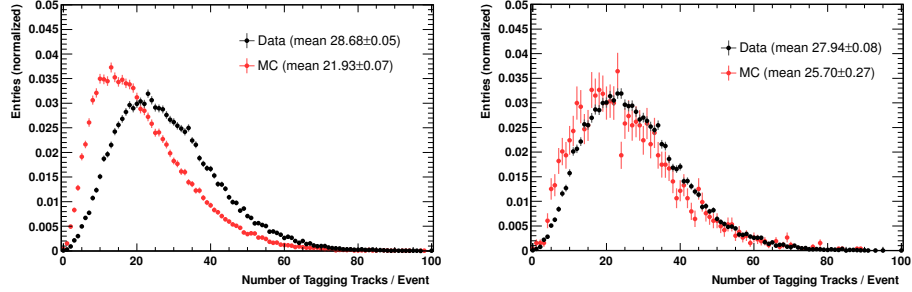


Figure 18: Number of Tagging Tracks per event without (left) and with (right) trigger requirements for data and MC simulation. With emulating the triggers the difference in the track multiplicity is reduced from 6.8 to 2.2 tracks per event.

Mean Number of Tagging Tracks per Event		
Trigger	Data	MC
none	28.68 ± 0.06	21.93 ± 0.07
L0	28.68 ± 0.06	25.84 ± 0.14
L0+Hlt1	28.74 ± 0.06	25.92 ± 0.22
L0+Hlt1+Hlt2	28.29 ± 0.07	25.92 ± 0.26
L0+Hlt1+Hlt2+TOS	27.94 ± 0.08	25.70 ± 0.27

Table 7: Mean number of Tagging Tracks the event for different trigger decision requirements.

The following trigger decisions are selected:

- L0: all possible trigger decisions
- HLT1: *TrackALL0*
- HLT2: *IncPhi*

Including all possible L0 trigger decisions, in data no additional events are rejected by this requirement. However in MC simulation 73.5% of the events are cut.

The *TrackALL0* trigger selects events with a requirement on Pt and the track quality. On HLT2 level the *incPhi* trigger decisions requires the presence of at least one reconstructed ϕ meson. For both data and MC simulation about 70% of the events which pass the HLT1 requirement also pass the *incPhi* trigger. In only choosing this one HLT2 trigger decision inconsistencies between data and MC simulation related to different trigger settings could be excluded. For the HLT1 and the HLT2 only events, which are triggered by the D_s^+ were selected to eliminate further possible inconsistencies. These trigger decision cuts decrease statistics in the MC simulation by 93%⁷ but also bring better agreement as shown in the following.

As described in section 2.2.3 the trigger selects especially high momentum tracks. Thus the D_s^+ momentum distribution is changed as seen in figure 17. Whereas without the trigger requirements the MC simulated D_s^+ transverse momentum is significantly softer than in data with using them it is nearly in agreement. This is important because with a high momentum D_s^+ also other particles from the fragmentation have access to higher energies. Thus in these events the Tagging Tracks should be better separated from the background.

Another quantity in which the improvement of using the trigger requirements is seen is the number of Tagging Tracks per event shown in table 7. Compared to data the surplus of in the mean 6.8 Tagging Tracks per event in MC simulation is reduced to 2.2 with the requirement of the trigger decisions. Furthermore also the shape of the Tagging Track multiplicity distribution (see figure 18) is also improved.

After this correction the remaining lower track multiplicity in MC simulation could have several reasons. On the one hand the MC generation could be wrongly described and thus for example the underlying event activity is underestimated. On the other hand the detector description could be insufficient. This will be investigated in the following.

All results presented in this chapter are obtained after applying the trigger requirements presented in this section.

⁷Events in MC with/without trigger requirements: 2635/36990.

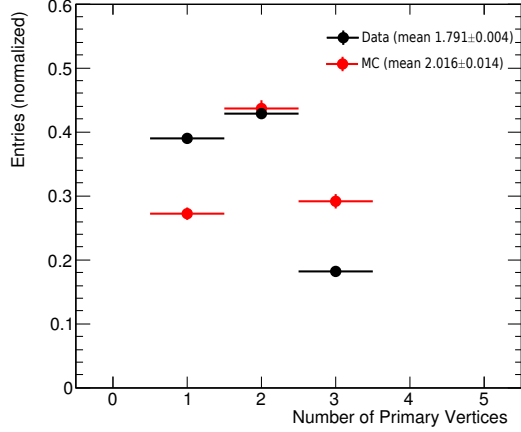


Figure 19: Number of primary vertices in data and MC simulation.

	Mean Number of Tagging Tracks				
	1 PV	2 PVs	3 PVs	1-3PVs	1-3PVs rw.
Data	30.78±0.13	27.12±0.11	23.79±0.16	27.94±0.08	27.94±0.08
MC	27.97±0.53	25.97±0.41	23.13±0.44	25.70±0.27	26.25±0.28
Difference	-9.1±1.8%	-4.2±1.6%	-2.8±2.0%	-8.02±1.0%	-6.1±1.0%

Table 8: Mean number of Tagging Tracks for different numbers of PVs in the event for data and MC simulation. In the rightmost column MC simulation is reweighted according to the number of PVs in data. With this the difference in track multiplicity reduces from 8% to 6%.

5.3.2 Primary Vertex Multiplicity

The beam parameters and thus the Primary Vertex (PV) multiplicity differs from the MC simulated one (see figure 19). In MC simulation there are in the mean 2.016 ± 0.014 PVs and in data 1.791 ± 0.004 PVs. This is corrected for by reweighting MC simulated events according to the data distribution. Each MC event receives a weight (a positive real number) corresponding to the ratio of the data distribution over the MC distribution. Thus the resulting distribution in MC simulation matches the one in data.

It is important to reweight the number of PVs as it is related to the track multiplicity in the event. With more PVs in the event there is a larger amount of background present. Due to the presence of other PVs less Tagging Tracks are assigned to the D_s^+ PV (see table 8).

Although the total number of tracks is disagreeing the dependency to the PV multiplicity is simulated well. An improvement of the Tagging Track multiplicity can be seen after reweighting according to the number of PVs.

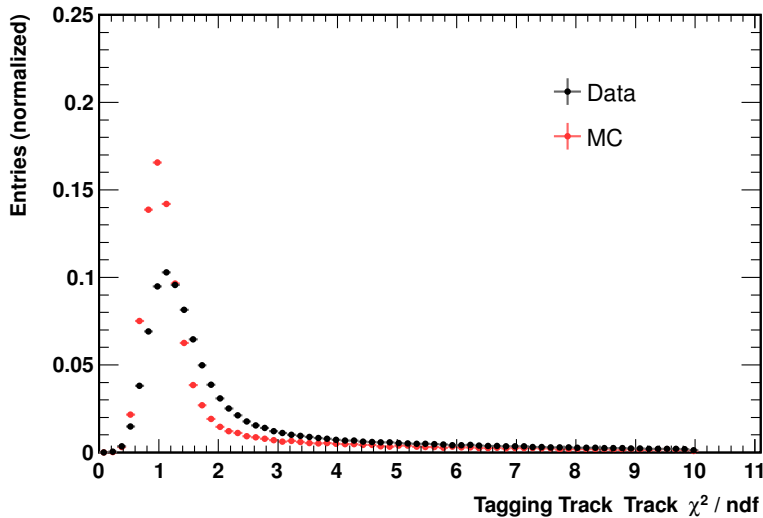


Figure 20: Tagging Track Track χ^2 divided by the number of degree of freedom distributions. The yet achieved Track resolution in data is still not reaching the one expected and used in the MC simulation. The tails of the distributions important for the SSKT however are in agreement.

In the following this reweighted MC simulation will be used. The effect on the mistag probability of the SSKT is:

$$\Delta\omega = \omega_{MC,corrected} - \omega_{MC} = -0.0088$$

The difference in the mistag probability between data and MC simulation is getting even larger with this correction. This indicates that the discrepancy is even worse than assumed in the first place.

5.3.3 Track Resolution

As the experiment is still in the initial data taking phase the detector has not yet reached its final precision. This is reflected in a worse mass and vertex resolution compared to MC simulation.

Concerning the Tagging Tracks this can be seen in the Track χ^2/ndf distribution shown in figure 20. It is expected to have a peak at one, like any χ^2 distribution but also have a long tail. The long tail of the distribution is due to a wrong assignment of hits in the track reconstruction or an uncorrected movement of a sub detector. In comparison to MC simulation the data Track χ^2/ndf distribution is not only shifted to the larger values but also broader. Nevertheless there is agreement in the tails, which is important for the SSKT. Favored in the SSKT is a loose cut on this value (the SSKT optimization will be discussed in appendix A). Cutting Track $\chi^2/\text{ndf} < 5$ there are only 3.9% of the Tagging Tracks in data and 3.6% in MC simulation after all SSKT cuts not passing this cut. Therefore it is assumed that inconsistencies in this variable are negligible.

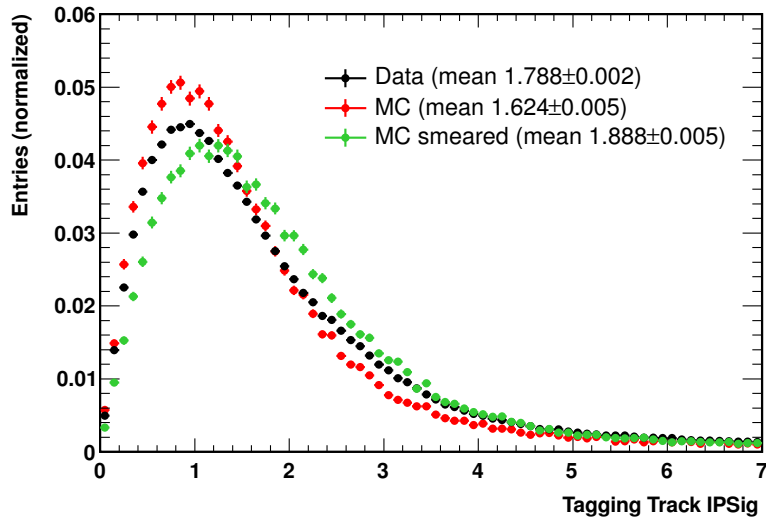


Figure 21: The IPSig distribution of Tagging Tracks for data and MC. In MC simulation the IP resolution is artificially worsened (smeared).

Furthermore the track resolution can be visualized by the IPSig distribution (see figure 21). As D_s^+ fragmentation tracks come directly from the PV this value should be small. Therefore as the distribution in MC simulation is narrower also a better tagging performance can be assumed. However with a loose SSKT cut ($IPSig < 5$) it can be expected that the effect on the mistag probability ω is only small.

To test this hypothesis the simulation is corrected for the worse resolution. The IP of the tracks in MC simulation is randomly altered (smeared). This procedure is described in detail in [27].

The algorithm overestimates the effect for the Tagging Tracks. However, even with an worse IPSig distribution than in data this sample could not explain the different ω in data and MC simulation.

Due to the change of the IP values different events are selected in the algorithm. This introduces an extra statistical fluctuation which is larger than the effect of changing the IPSig itself. To eliminate this fluctuation only events are regarded which were present in both the corrected and uncorrected sample⁸. This is the case for 88% of the events from the original sample.

The result is that the effect on the SSKT is negligible:

$$\Delta\omega = \omega_{MC,smeared} - \omega_{MC} = + 0.0012$$

⁸It was checked if the events had the same ID (event number).

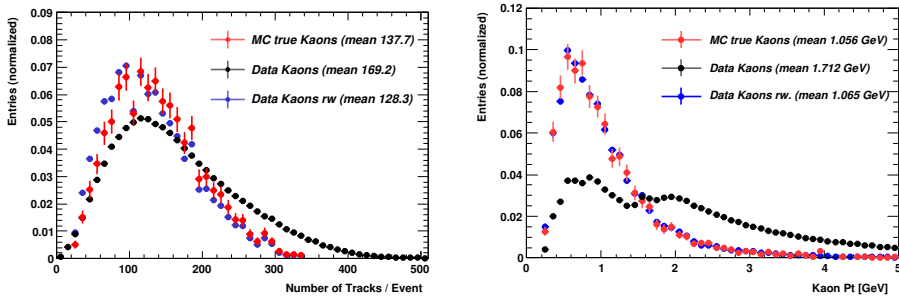


Figure 22: Number of tracks in the event(left) and the true kaon transverse momentum distribution(right) for the MC simulation and data. Data is reweighted first in the number of tracks and then simultaneously in P and η . Afterwards also the kaons P_t distribution is in agreement.

5.3.4 Particle Identification

Particle Identification (PID) which was explained in section 2.2.2 is important for the SSKT. It is necessary to reject the large amount of pions and protons which would otherwise interfere in the SSKT algorithm. In the following the PID performance of the LHCb detector on data is compared to the simulation. In the last part of this section its effect on the mistag probability is derived.

The tracks in an event are mainly pions, kaons and protons with the relative fractions 22:5:2⁹. The effect of other particles (4.25%) can be neglected for this analysis. Thus the PID performance measurement can be split up into two parts. First there is the kaon identification efficiency and secondly there is the probability for identifying protons and pions as kaons (MisID probability).

To measure the PID performance on data, DLL distributions of kaons, pions and protons from different resonances obtained with the $sPlot$ technique[31] were provided[30]. The used data sample was recorded in 2010, thus in the same data taking periods as also the D_s^+ data sample were written.

In MC simulation the generator level information was used to identify the particles. From the Tagging Tracks the true kaon, pion and proton subset is respectively looked at.

The PID performance is calculated for a specific set of DLL cuts. The cuts chosen in the SSKT are $DLL_{kpi} > 5$ and $DLL_{kp} > -5$. Dividing all kaons passing a DLL cut by all of the kaons in the sample gives the kaon PID efficiency. Analogously the pion/proton MisID is calculated by all the pions/protons which pass the DLL cut divided by all pions/protons.

To compare DLL distributions of data and MC simulation the particles in both samples have to cover the same phase space. For example the

⁹This information was received from MC.

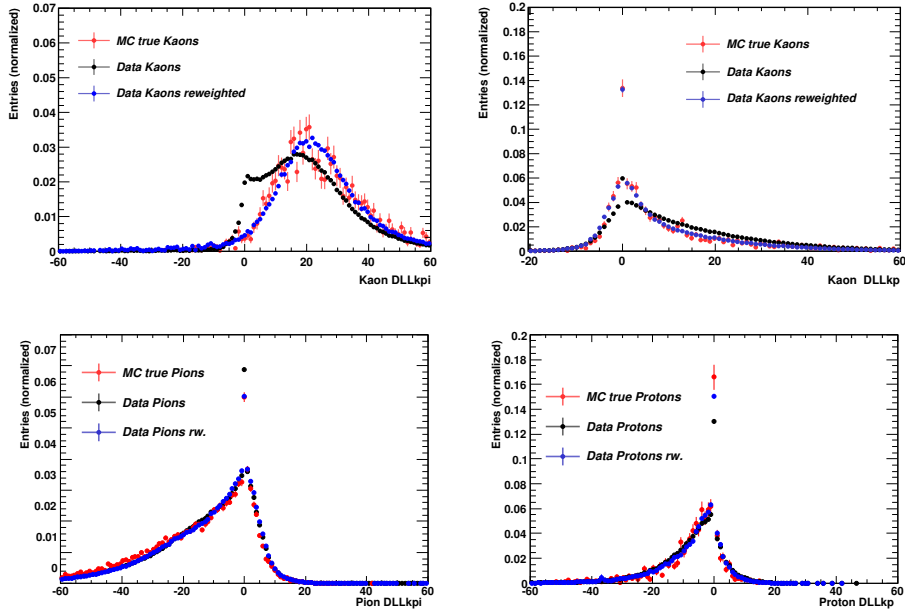


Figure 23: DLL distributions of kaons (top), pions (bottom left) and protons (bottom right) for MC simulation and data. After reweighting data to MC simulation there is good agreement.

transverse momentum of kaons in the PID test data sample is larger than the momentum of the Tagging Tracks (see figure 22).

Particles from the data samples are reweighted according to properties of the MC Tagging Tracks. At first the mean number of total tracks in the event is reweighted, as it is assumed to be uncorrelated to the track properties. More tracks in the event would result in a higher occupancy in the RICH detectors. Thus the PID performance is worse as it is more difficult to select for each track the corresponding ring in the RICH detectors.

Afterwards the pseudorapidity and the momentum of the tracks are reweighted simultaneously, as the RICH performance depends on the direction and momentum of a particle. The phase space for which enough statistics is available to do this reweighting is:

- Kaons: $P [7\text{GeV}, 40\text{GeV}]$, $\eta [2.5, 4.2]$, $P_t < 5\text{GeV}$
- Pions: $P [2\text{GeV}, 40\text{GeV}]$, $\eta [2.5, 4.5]$, $P_t < 5\text{GeV}$
- Protons: $P [7\text{GeV}, 40\text{GeV}]$, $\eta [2.5, 5.0]$, $P_t < 5\text{GeV}$

These regions covered the phase space of 74% of the Tagging Tracks after the SSKT cuts and thus they are assumed to be representative.

The DLL distributions after reweighting can be seen in figure 23. The corresponding efficiencies are listed in table 9. The PID performance in MC simulation is slightly better than for data. The kaon efficiency is higher for both DLLkpi and DLLkp, whereas the probability for identifying pions

PID Performance for Kaons, Pions and Protons

	MC	Data
Kaon Efficiency for $DLLkpi > 5$	$93.7 \pm 0.5\%$	$91.2 \pm 0.3\%$
Pion MisID Probability for $DLLkpi > 5$	$5.56 \pm 0.14\%$	$7.24 \pm 0.03\%$
Kaon Efficiency for $DLLkp > -5$	$96.2 \pm 0.4\%$	$94.6 \pm 0.1\%$
Proton MisID Probability for $DLLkp > -5$	$55.6 \pm 0.1\%$	$56.1 \pm 0.03\%$

Table 9: PID performances for data and MC simulation.

and protons as kaons is lower. However, the differences are only on the 1-2 percent level and therefore the PID performance cannot be expected to be the reason for the discrepancy in the tagging efficiency between data and MC simulation.

This too high PID performance in the MC simulation is corrected by artificially worsening the $DLLkpi$ and $DLLkp$ cuts.

$$100 \cdot \left(1 - \frac{Data\,PID\,Eff}{MC\,PID\,Eff} \right) \%$$

of the true kaons which passes the $DLLkpi$ and $DLLkp$ cuts are cut in addition. Analogously

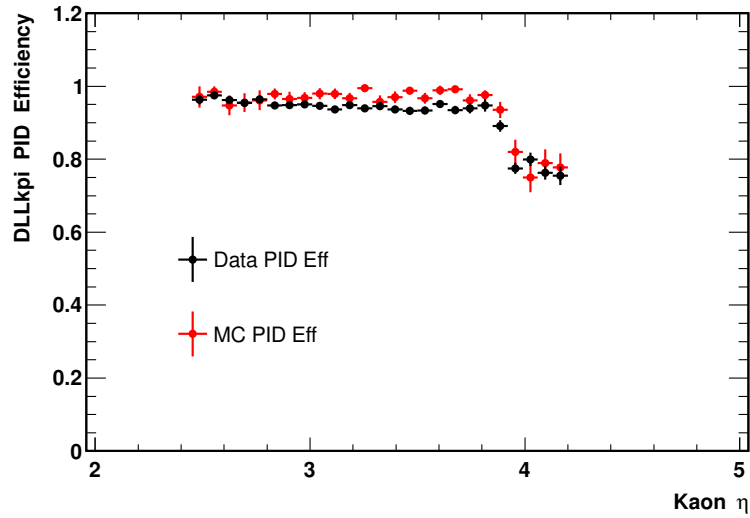
$$100 \cdot \left(1 - \frac{1-Data\,MisID}{1-MC\,MisID} \right) \%$$

of the true protons and pions, which would have been cut by the respective DLL cut, are not cut. The PID efficiency is correlated to the momentum and pseudorapidity of the particles. Thus this correction could be varying in different phase space regions. However it is found out that these correction factors do not change in phase space significantly. This is checked for different p , p_t and η bins. An example of this study is shown in figure 24. Therefore this correction is done with phase space independent correction factors. As a systematic study also a worst case scenario is simulated overestimating the effect by 100%.

As expected the effect on the mistag probability is negligible:

$$\Delta\omega = \omega_{MC,worse\,PID} - \omega_{MC} = + 0.0015$$

$$(\text{worst case scenario } \Delta\omega = + 0.0026)$$



S

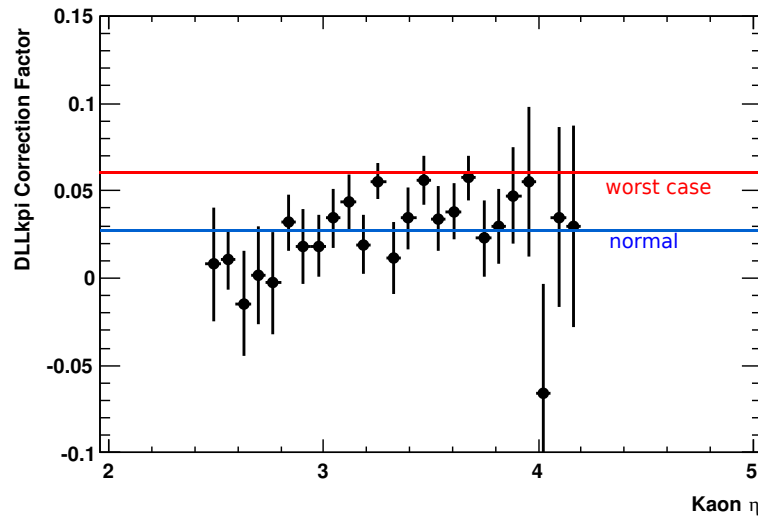


Figure 24: Top: The PID efficiency for kaons from data and MC simulation for different η values. Bottom: The corresponding MC correction factors for the different η bins. The corrections factors agree in all bins with the used factor (blue) and are always smaller as the hypothetical worst case overestimating the effect by 100% (red).

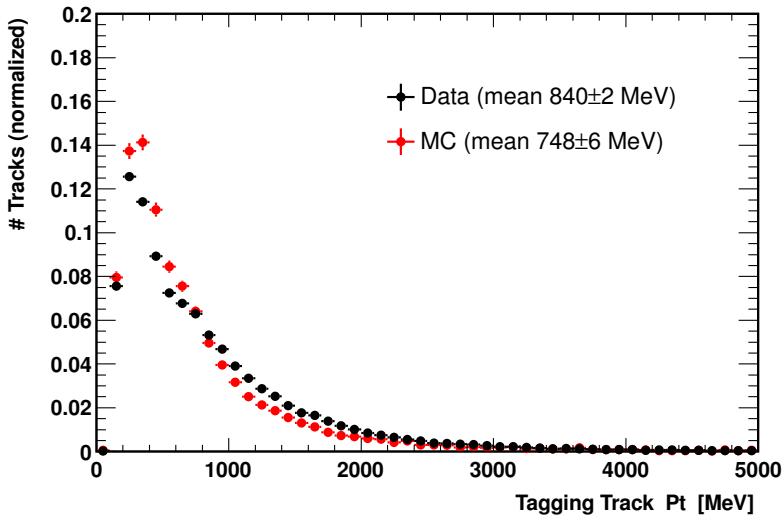


Figure 25: Tagging Track transverse momentum distribution for data and MC simulation. Additional cuts applied are $\text{TrChi2} < 5$, $\text{IPSig} < 5$ and $\text{DL-Lkpi} > 5$. The plots are scaled to 1.

5.3.5 Underlying Event

After looking at possible detector effects the remaining discrepancy in the total Tagging Track multiplicity is assumed to be related to an incorrect description of the Underlying Event (UE). The contribution of the D_s^+ fragmentation on the total number of tracks would be too small. Looking at MC simulation there are 0.57 ± 0.02 tracks per event from the D_s^+ fragmentation and in total 26.25 ± 0.28 tracks per event. Compared to data 1.69 Tagging Tracks are missing which is about three times the amount of D_s^+ fragmentation tracks which can be therefore be excluded to be the reason for this discrepancy.

However not only is there a different UE activity but its tracks also have a different transverse momentum spectrum (see figure 25). Therefore the difference in the track multiplicity depends on the momentum cuts applied on the Tagging Tracks sample. To study the effect on the SSKT performance in the following all SSKT cuts (see table 15) are applied for this study. Only the variable $\Delta\phi$ and ΔQ are not cut, as they are correlated to each other and $\Delta\phi$ is the variable of interest for this analysis.

The Tagging Track $\Delta\phi$ distribution can be seen in figure 26. Tracks from the UE are assumed to be uncorrelated to the D_s^+ decay and thus have a flat $\Delta\phi$ distribution. The tracks from the D_s^+ fragmentation are expected to have a peaking distribution in the smaller $\Delta\phi$ region as can be seen in figure 13 in section 4.1. Therefore in the region $\Delta\phi > 1$ dominantly tracks from the UE can be found. Due to momentum conservation in the $c\bar{c}$ pro-

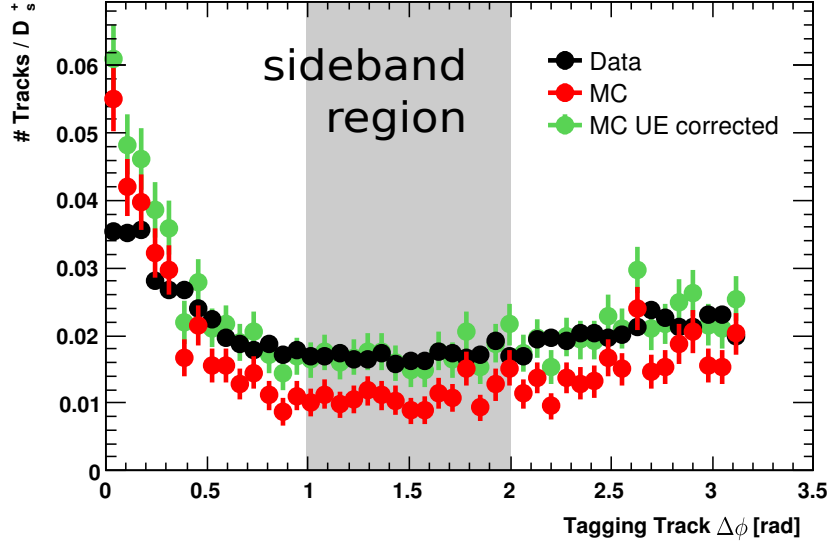


Figure 26: Tagging Track $\Delta\phi$ distribution of data and MC simulation with all SSKT cuts. In MC simulation artificial background is introduced which is scaled in the sideband region $\Delta\phi$ [1,2].

duction the opposite D predominantly flies into the opposite ϕ direction¹⁰. Therefore in the region $\phi > 2$ a rise in the number of tracks is present. This is the reason for also excluding this region in the following.

Measuring the amount of tracks in the $\Delta\phi$ sideband region [1,2] there are about $35.5 \pm 3.8\%$ too few tracks in MC simulation.

This could explain a worse tagging performance. In the following the impact on the SSKT of an artificial enhancement of the UE by this factor is first calculated and afterwards simulated. Omitting the ΔQ cut will be treated as a systematic uncertainty, whereas the $\Delta\phi$ cut is applied after this measurement.

Theoretical change in ω due to a lower activity of the UE

After the SSKT cuts the Tagging Track with the highest Pt is used for determining the D_s^+ tagging decision (see section 4.1). Thus the additional background from the UE could affect the SSKT in three different ways:

- the D_s^+ has already a tag and the additional track is ignored
- the D_s^+ has already a tag and the additional track replaces this tag
- the D_s^+ has no tag yet and the additional track creates a new tag

The ratios of these contributions are studied to determine the expected effect on the mistag probability. The majority of $73.4 \pm 1.8\%$ of the D_s^+ in

¹⁰This was checked in MC simulation.

MC simulation have no Tagging Tracks left after all SSKT cuts and thus are untagged. Therefore it is concluded that the last point outweighs the others. The effect of the first two points is handled as a systematic.

With these assumptions each added Tagging Track passing the SSKT cuts would in approximation lead to an additional tagged D_s^+ . The tag of this new D_s^+ would be either wrong or right in 50% of the cases. Thus to calculate the change in ω one has to add to the number of all already tagged D_s^+ $100 \cdot x\%$ more D_s^+ . Where x is the number of additional tagged D_s^+ divided by all already tagged D_s^+ . After the cuts in the MC simulation there are in average 0.311 tracks per event and due to a lower UE activity there would be 0.078 tracks missing. Thus: $x = 0.078/0.311$.

Because of 50% of the additional tagged D_s^+ would have a wrong tag the number of wrong tagged D_s^+ has to be increased accordingly. With $n_{wrongTag}$ and n_{allTag} the number of corresponding D_s^+ and

$$\omega = \frac{n_{wrongTag}}{n_{allTag}}$$

the change in the mistag probability is:

$$\begin{aligned} \Delta\omega(x) &= \omega_{MC+UE} - \omega_{MC} = \frac{n_{wrongTag} + 0.5 \cdot x \cdot n_{allTag}}{n_{allTag} + x \cdot n_{allTag}} - \frac{n_{wrongTag}}{n_{allTag}} \\ &\Rightarrow \Delta\omega(x) = (0.5 - \omega_{MC}) \frac{x}{1+x} \end{aligned} \quad (1)$$

The systematic uncertainty of this calculation is based on mainly two aspects. Omitting the ΔQ cut there is a worse ω in data of 0.025 and in MC of 0.033. The difference between this two effects is handled as the systematic uncertainty on ω . On the other hand the maximal possible influence of the 27% already tagged D_s^+ is calculated. The two extremes are that either these additional Tagging Tracks would be all ignored or would all replace a right tag.

The effect of additional UE on ω for the present values would be:

$$\Delta\omega_{theo}(x = 0.251) = + 0.0367 \pm 0.0033 \text{ (stat.) } \begin{matrix} +0.0036 \\ -0.0091 \end{matrix} \text{ (syst.)}$$

This is the dominating effect compared to the other ones observed until now. It could explain a large part of the different tagging performance between data and MC simulation. However it could not account for the whole difference in the tagging performance. This indicates that there is possibly still another effect responsible for the discrepancy in the tagging performance.

Tagging Efficiency ϵ	
data	0.266 ± 0.003
MC	0.255 ± 0.009
MC with additional background	0.306 ± 0.009

Table 10: Tagging efficiency ϵ for data and MC simulation with additional simulated background from the UE. Due to a higher track multiplicity ϵ is also enhanced and MC simulation is no longer in agreement with data.

Simulating missing UE with minimum bias data

The missing UE activity is corrected for using minimum bias data, which are data samples containing only background events. From an independent minimum bias MC10 sample Long Tracks are extracted. The IPSig from the original PV is used and other track properties are calculated in the same way as for real Tagging Tracks. The amount of additional tracks is scaled to achieve agreement in the number of tracks of data and MC simulation in the $\Delta\phi$ sideband (see figure 26). The track multiplicity in this region is 0.242 ± 0.003 in data, 0.156 ± 0.009 in MC simulation and 0.243 ± 0.011 in MC simulation with the additional min bias tracks. As a systematic study the additional UE is varied by 10%.

As seen in the theoretical part of this analysis the transverse momentum of the Tagging Tracks must agree, as the one with the highest Pt is used to calculate the tagging decision. This is however the case as can be seen in figure 27. The change in the mistag probability is in agreement with the theoretical expected one:

$$\Delta\omega_{sim} = + 0.0326\pm 0.0046$$

Besides ω another aspect becomes important. Although the default tagging efficiency ϵ is similar for data and MC simulation this is no longer the case with this correction (see table 10) . In MC simulation it raises up by 0.05 and is therefore now significant larger as data.

Hence it can be assumed that a different UE activity is not the only reason for the discrepancy in the tagging performance of data and MC simulation. The effect in the mistag probability is too small compared to the observed difference of $\omega_{MC} - \omega_{Data} = 0.062\pm 0.020$. Furthermore the different tagging efficiency can no longer be explained by a statistical fluctuation. A possible solution would an additional incorrect description of the D_s^+ fragmentation in Pythia as shown in the next section.

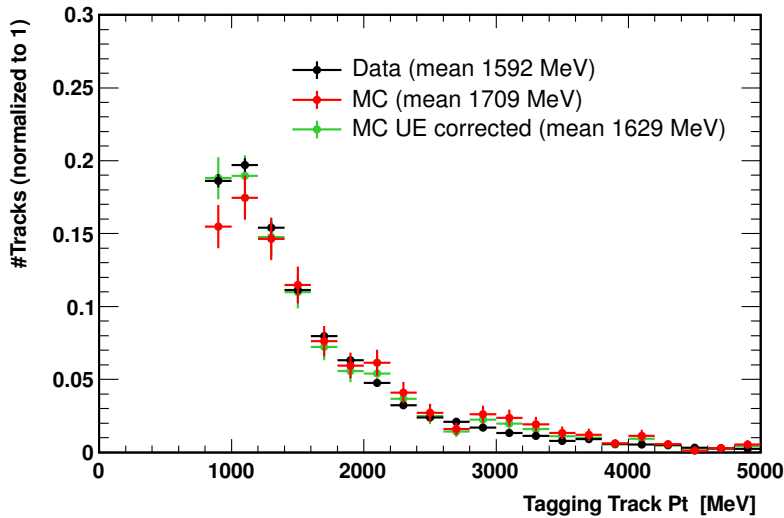


Figure 27: Tagging Track Pt distribution after all SSKT cuts but ΔQ for data, MC and MC the with additional simulated background. The transverse momentum which is important for the SSKT is in agreement.

5.3.6 Fragmentation

As shown in the last section a different activity in the Underlying Event (UE) between data and MC simulation could be corrected using additional minimum bias data. It could be scaled to the total number of tracks if the D_s^+ fragmentation is described correctly. However, there would be no possibility to scale the D_s^+ fragmentation, though. A new MC simulation sample with a new tuning would have to be created.

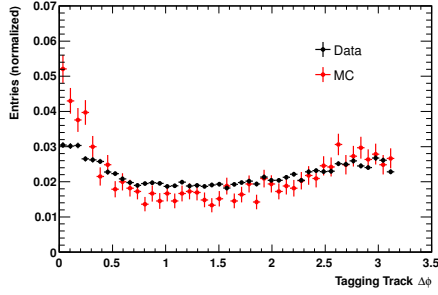
Having an unbiased look at the D_s^+ fragmentation is rather difficult. Detector and track reconstruction effects have to be understood. Any cut which suppresses background will also alter the D_s^+ fragmentation track distributions and question if not only this cut is the reason for possible discrepancies.

To enhance the ratio of D_s^+ fragmentation tracks additional cuts are applied to the Tagging Tracks. The momentum is assumed to be described correctly and thus it is cut very hard ($Pt > 900$ MeV). Further cuts are done on the impact parameter ($IP_{Sig} < 5$) and the PID ($DLL_{pi} > 5$), as these variable was checked in 5.3.3 and 5.3.4.

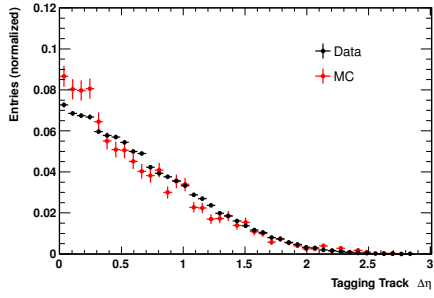
The D_s^+ fragmentation tracks are best seen in the $\Delta\phi$, $\Delta\eta$ and ΔQ distributions as shown in figure 28.

Comparing to figure figure 13 from section 4.1 they are expected to be present in each plot at lower values. These are however exactly the regions where the shape of data and the MC simulation is diverging in a way that there are too many tracks in MC simulation.

Tagging Track $\Delta\phi$



Tagging Track $\Delta\eta$



Tagging Track ΔQ

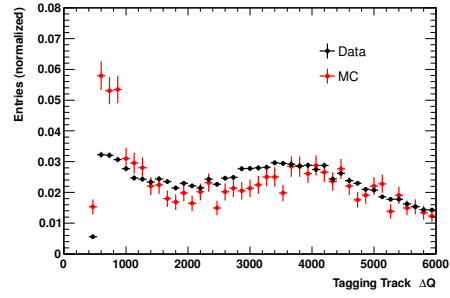


Figure 28: Tagging Track $\Delta\phi$, $\Delta\eta$ and ΔQ distribution for data and MC. The plots are normalized to 1. Additional cuts applied are $P_t > 900$ MeV, $IP_{Sig} < 5$, $DLL_{kpi} > 5$. There is a discrepancy between data and MC simulation exactly in the regions where D_s^+ fragmentation tracks are expected.

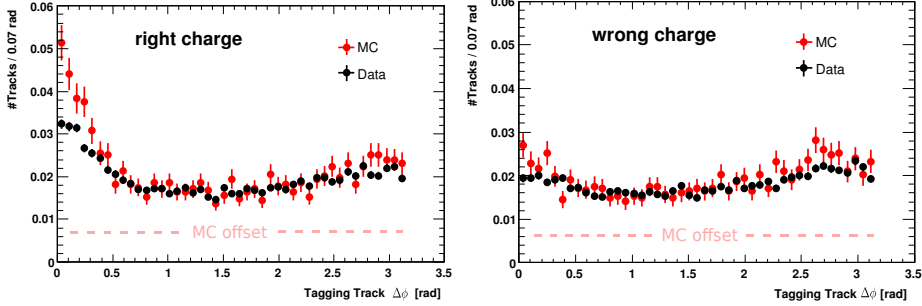


Figure 29: Tagging Track $\Delta\phi$ distribution. MC simulation is corrected for missing UE activity with artificial background (flat distribution). The tracks are divided into those with the right and wrong charge with respect to the tagging decision.

$\Delta\phi$ plot with UE correction

The discrepancy between data and MC simulation can best be visualized in the Tagging Track $\Delta\phi$ plot. As explained in the last section tracks from the UE are assumed to have a flat $\Delta\phi$ distribution. In contrast particles from the D_s^+ fragmentation are expected to be located predominantly at smaller $\Delta\phi$ values. Thus the different UE activity is corrected by adding a flat offset to the MC simulation $\Delta\phi$ distribution¹¹. This offset is scaled in a way that there is agreement in the number of Tagging Tracks in the region $\Delta\phi$ 1-2. The remaining difference at smaller $\Delta\phi$ values is interpreted as an effect of the D_s^+ fragmentation.

To use a feature available in the D_s^+ system this is done separately for the right and for the wrong charged tracks with respect to the tagging decision. As discussed in section 4.1 the particles from the D_s^+ fragmentation tracks should in majority have right charge. This behavior is seen in figure 29. There is a sharp increase in $\Delta\phi < 0.5$ for the right charged Tagging Tracks and also a little increase for the wrong charged ones.

The distributions of data and MC simulation agree in most $\Delta\phi$ regions. However, for right charged tracks with $\Delta\phi < 0.5$ the track multiplicity in MC simulation is significantly higher than in data. Also for the wrong charged tracks a discrepancy can be seen, here. This is also the place where the majority of D_s^+ fragmentation tracks are expected.

¹¹In contrast to using the corrected MC simulation sample from the last section this method avoids additional statistical fluctuations.

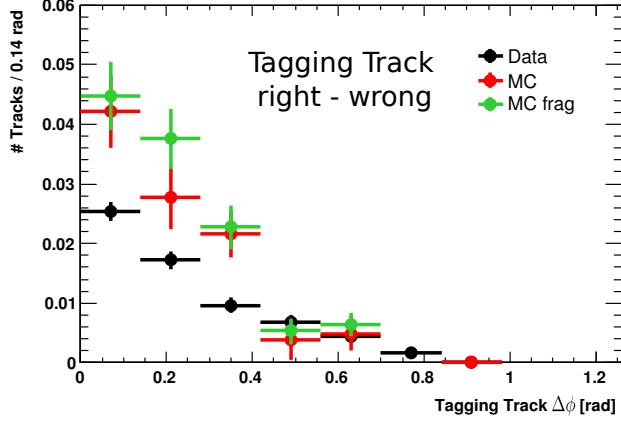


Figure 30: $\Delta\phi$ distribution of Tagging Tracks from D_s^+ fragmentation with all SSKT cuts. *Data* and *MC* is constructed by subtracting the wrong charged from the right charged tracks. *MC Frag* are additionally only tracks from the D_s^+ fragmentation. There are significant more tracks in MC simulation than in data.

Having agreement after the UE correction in all but this region strongly indicates that it is an incorrect description of the D_s^+ fragmentation which is the reason for the remaining discrepancy in the tagging performance.

Direct Look at Fragmentation

Furthermore there is the possibility to have a direct look at the D_s^+ fragmentation. Subtracting the distribution of the wrong charged Tagging Tracks from the right charged ones is assumed to show only the corresponding difference of the D_s^+ fragmentation tracks. In figure 30 this distribution is shown for the Tagging Tracks after all SSKT cuts.

With subtracting the wrong charge tracks the background from the UE is canceling as its charge is independent from the D_s^+ . Thus the amount of remaining tracks should be the surplus of right charged D_s^+ fragmentation tracks with respect to the wrong charged ones.

Charge asymmetry effects of the detector does not affect this distribution as there is the same amount of D_s^+ and D_s^- in the data samples. It is checked that tracks from the signal D_s^+ decay are not interfering either. A small systematic uncertainty is introduced by tracks coming from the decay of the opposite D . According to MC simulation 4% of the tracks passing all SSKT cuts come from an decay of the opposite D .

As a cross check in MC simulation this distribution is also plotted for Tagging Tracks with the requirement to be a true D_s^+ fragmentation track. Within statistics this distribution agrees with the original one of MC simulation.

However comparing the MC simulation to data there is a large discrepancy of in total 0.037 ± 0.011 tracks, which corresponds to a surplus of $36.9 \pm 7.1\%$ of right charged D_s^+ fragmentation tracks in MC simulation.

As outlined above this is assumed to be because of too many tracks from the D_s^+ fragmentation in MC simulation.

Effect on Mistag Probability

The effect on the mistag probability if these 0.037 ± 0.011 tracks would be removed in MC simulation is calculated. Only 16% of the tagged D_s^+ have more than one Tagging Track left after the SSKT cuts. Thus in an approximation removing a Tagging Track would be equal to remove the tag of the corresponding D_s^+ . Furthermore all of these 0.037 ± 0.011 tracks have the right charge and therefore the number of all tagged D_s^+ (n_{allTag}) is reduced accordingly. A change in the amount of wrong charged D_s^+ fragmentation tracks ($n_{wrongTag}$) is not examined in this study for which reason the total number of wrong tagged D_s^+ ($n_{wrongTag}$) remains the same. With the ratio of the amount of reduced D_s^+ fragmentation tracks

$$y = \frac{\text{reduced frag tracks}}{\text{all tracks}} (= \frac{0.037}{0.269})$$

and

$$\omega = \frac{n_{wrongTag}}{n_{allTag}}$$

the effect on the mistag probability is:

$$\begin{aligned} \Delta\omega(y) &= \omega_{MC-Frag} - \omega_{MC} = \frac{n_{wrongTag}}{n_{allTag} - y \cdot n_{allTag}} - \frac{n_{wrongTag}}{n_{allTag}} \\ &\Rightarrow \Delta\omega(y) = \omega_{MC} \left(\frac{y}{1-y} \right) \end{aligned} \quad (2)$$

For the present values this would result in:

$$\Delta\omega(y = 0.137) = + 0.056 \pm 0.018(\text{stat.})$$

Analogously the effect on the tagging efficiency ϵ can be calculated. With n_{all} the number of all D_s^+ in the sample it is:

$$\Delta\epsilon(y) = \epsilon_{MC-Frag} - \epsilon_{MC} = \frac{n_{allTag} - y \cdot n_{all}}{n_{all}} - \frac{n_{allTag}}{n_{all}} = -\epsilon_{MC} \cdot y$$

The tagging efficiency ϵ would be reduced to 0.263 ± 0.075 which would be again comparable to data ($\epsilon_{Data} = 0.266 \pm 0.003$). Thus the effect of additional UE resulting in an increase of epsilon would be compensated.

Compared to the other corrections removing D_s^+ fragmentation tracks has the largest effect on ω . Together with the different activity of the UE as discussed in section 5.3.5 it could explain the different ω observed between data and the MC simulation. Furthermore also ϵ would be in agreement.

5.4 Summary

A different tagging performance was observed between data and MC simulation. Multiple properties of MC simulation which could have an effect on tagging were studied and corrected if necessary. Besides others the trigger was emulated, the number of primary vertices was reweighted, the track impact parameter was smeared, the particle identification was worsened and also random tracks were introduced simulating additional underlying event activity. The effect of these corrections on the mistag probability ω of the SSKT is shown in table 11. Most corrections have only a small influence on the tagging performance and change ω only little and in both directions. The largest effects are the enhancement of the underlying event activity by 35.5% and removing 36.9% of the D_s^+ fragmentation tracks in the phase space region used by the SSKT. Altogether the observed difference in ω and the original agreement in the tagging efficiency ϵ between data and MC simulation can be explained by these two corrections.

Corrections in MC	Effect on ω
primary vertex multiplicity	- 0.009
track impact parameter	± 0.001
PID performance	+ 0.002 (max + 0.003)
underlying event	+ 0.037 \pm 0.003 (stat.) $^{+0.0036}_{-0.0091}$ (syst.)
D_s^+ fragmentation	+ 0.056 \pm 0.018(stat.)
in total	+ 0.086
observed difference	
between data and MC	+ 0.062 \pm 0.020

Table 11: Effects of corrections on MC simulation on the mistag probability ω . The observed difference can be explained.

6 Performance of the Same Side Kaon Tagger for B_s^0 mesons

After having examined the Same Side Kaon Tagger (SSKT) on D_s^+ decay, the SSKT is studied on B_s^0 decay in this chapter. Due to the oscillation of B_s^0 mesons it is more difficult to investigate the tagger in this system. The flavour content of the B_s^0 changes before its decay and thus a direct check of the tag is not possible.

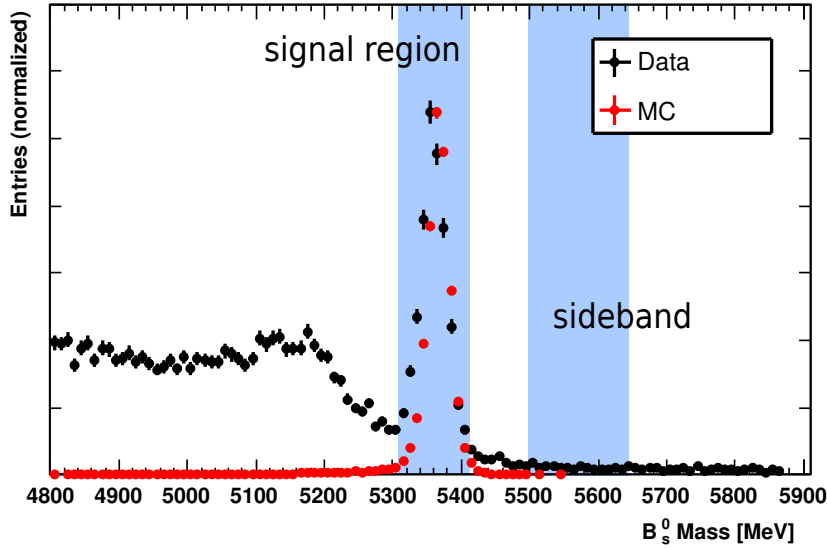


Figure 31: B_s^0 mass distribution. The peak and sideband region are highlighted. The sideband was scaled by fitting an exponential function to the background.

To determine the B_s^0 oscillation frequency the flavour content of the meson have to be measured time dependently. At decay time the flavour is determined by the charge of the B_s^0 decay products. It is the flavour taggers which provide information about the production flavour of these mesons.

The performance of the SSKT could be studied on the similar D_s^+ system. The MC simulation of the D_s^+ and B_s^0 system should be similar in many points. The description of the detector response and its efficiencies should be comparable. The UE should behave for both particle decays in the same way. However, the fragmentation and the covered phase space of particles should be different. Hence the results obtained in the last chapter cannot be directly compared to the results of this chapter. Nevertheless, as both MC simulations have much in common, it can be expected that similar effects are present and similar corrections are necessary.

In this chapter the SSKT performance for the B_s^0 mesons will be compared between data and the MC simulation. The tools tested in the D_s^+ system

will be applied. The same quantities of the detector simulation and MC generation will be compared and differences will be corrected in MC simulation. A remaining discrepancy will be tried to be traced back to the MC generation itself.

6.1 B_s^0 Selection

The data-set used in this chapter contains the first 341 pb^{-1} recorded 2011 at LHCb. The center of mass energy was $\sqrt{s} = 7 \text{ TeV}$.

The event selection can be seen in table 12. Only events with exactly one reconstructed B_s^0 are selected. Low occupancy events are selected by requiring less than 150 Long Tracks. Several trigger decisions are available. Concerning the L0 trigger again all possible trigger decisions are used. The *TrackALL0* trigger from the HLT1 has a requirement on Pt and the quality of tracks. In the *incPhi* trigger events with at least one reconstructed ϕ meson are selected. The *topoXbody* trigger combines generically X tracks and searches for high momentum particles.

Event Selection	
Number of B_s^0	1
Number of Long Tracks	< 150
L0 Trigger Decisions	- all -
HLT1 Trigger Decisions	<i>TrackALL0</i>
HLT2 Trigger Decisions	<i>incPhi, topo2body, topo3body, topo4body</i>

Table 12: Event selection for B_s^0 sample

The B_s^0 selection which is adapted from [28] is shown in table 13. The selected decay is $B_s^0 \rightarrow D_s^- (\phi \pi^-) \pi^+$ exploiting the D_s^- as well as the ϕ resonance. With momentum (P) and transverse momentum (Pt) cuts on the B_s^0 , D_s^- and their daughters dominantly high energetic B_s^0 are selected. High momentum tracks are better reconstructed and the low momentum background is reduced. A cut on the quality of the track fit (Track χ^2/ndf) ensured that only well reconstructed tracks are used. With DLL cuts it is assured that kaons are distinguished from pions. The B_s^0 decay particles are due to the large B_s^0 lifetime supposed to be well separated from the PV. Therefore a cut on the IPSig of the B_s^0 daughters is applied. The matching of the daughters into first the D_s^- and then the B_s^0 is assured by the Vertex χ^2 cut. The B_s^0 and D_s^- decay vertex are required to be separated from the PV with a cut on the PV separation significance. It is checked that the flight direction of the B_s^0 from the PV to its decay vertex is in agreement with the direction of its reconstructed momentum vector. This is done with a cut on $\cos\Theta$, which is the cosine of the angle between the flight direction and the momentum vector.

B_s^0 Selection	
only $B_s^0 \rightarrow D_s^- (\rightarrow \phi (\rightarrow K^+ K^-) \pi^-) \pi^+$ (and c.c.)	
D_s^- Mass	1969 ± 30 MeV
ϕ Mass	1019.5 ± 13 MeV
P	> 2 GeV
Vertex χ^2	< 12
$\cos\Theta$	> 0.9999
PV separation significance	> 64
D_s^-	
Pt	> 2 GeV
Vertex χ^2	< 12
IPSig	> 3
PV Separation Significance	> 100
D_s^- daughters	
P	> 2 GeV
Pt	> 300 MeV
IPSig	> 3
Track χ^2	< 5
DLLkpi	> -10 (for kaons), < 10 (for pions)
π^+ from B_s^0	
P	> 5 GeV
Pt	> 0.5 GeV
IPSig	> 3
Track χ^2	< 5
DLLkpi	< 5

Table 13: B_s^0 Selection used to separate signal B_s^0 from background.

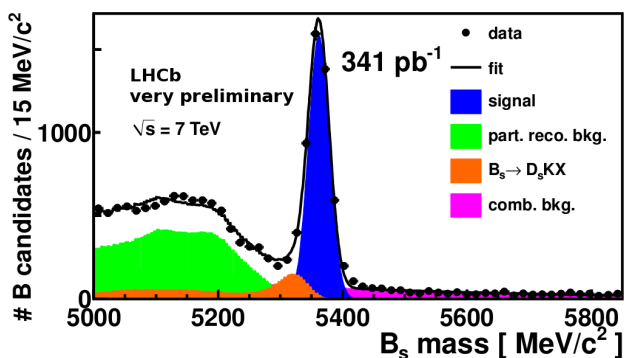


Figure 32: Fit of the B_s^0 mass for the decay $B_s^0 \rightarrow D_s^- (\phi \pi^-) \pi^+$ done in [28]. In the signal region only combinatorial background must be regarded. $B_s \rightarrow D_s K X$ can be treated as signal.

The resulting B_s^0 mass distributions can be seen in figure 31. In the MC simulation only the signal decay and no background is simulated. Therefore there is the need of a good handling of the background in data.

It was shown[28] that for the $B_s^0 \rightarrow D_s^- (\phi \pi^-) \pi^+$ decay channel and a similar selection only combinatorial background and misidentified $B_s^0 \rightarrow D_s^- K^+ X$ decays are present in the signal window (see figure 32). In $B_s^0 \rightarrow D_s^- K^+ X$ decays the bachelor kaon is misidentified as pion and thus also this decay passes the here presented B_s^0 selection. The decay can be handled as signal as the mass shift due to the wrong reconstruction is not changing the measured B_s^0 lifetime significantly. Therefore it can be assumed that for this decay channel only combinatorial background is present. This can be handled by sideband subtraction which was explained in section 5.1. A tight signal region from 5310-5410 MeV ($\pm 3\sigma$) is selected to suppress the influence of background in this study. The combinatorial background has a bended shape and therefore an appropriate scaling of the sideband has to be calculated. The background above 5500 MeV is fitted with an exponential function which is extrapolated into the signal region. It is deduced that a proper sideband is sized from 5500 to 5645 MeV. The signal yield of reconstructed B_s^0 signal candidates in the signal region has been determined to be 15180 in MC simulation and 4387 in data.

The Tagging Track selection (see table 14) is similar to the one used in the D_s^+ analysis. An additional Track χ^2/ndf cut is applied as this quantity was no problem in the D_s^+ system (see section 5.3.3). Due to the different trigger and event selection the amount of Tagging Tracks and also their distributions will not be directly comparable to the ones of section 5. Furthermore the tracks coming from the B_s^0 fragmentation are expected to be in a different phase space region than the ones coming from the D_s^+ fragmentation (see section 3.2.2). The cuts for the SSKT used in the following to measure

Tagging Track Selection	
Track Type	Long Tracks
Track χ^2	< 5
IPSig to D_s^+ PV	$<$ IPSig to any other PV
IPSig to any other PV	> 3
$\Delta\phi$ (track \leftrightarrow D_s daughters)	> 0.015
θ (track \leftrightarrow beam pipe)	> 0.012

Table 14: Tagging Track selection used to select tracks potentially interesting for the SSKT.

SSKT Cuts	
P	> 5250 MeV
Pt	> 750 MeV
IPSig	< 4.125
Track χ^2/ndf	< 3.75
$\Delta\eta$	< 0.525
$\Delta\phi$	< 0.7
ΔQ	< 1600
DLLkpi	> 4.5
DLLkp	> -8.5

Table 15: Default cuts for the B_s^0 SSKT algorithm. The tagging performance will be calculated based on these SSKT cuts.

the tagging performance are listed in table 15. They are the default B_s^0 SSKT cuts which are used also in other analyses at LHCb.

6.2 Default Tagging Performance

The SSKT is run on B_s^0 data and MC simulation with the selection described above and the tagging power (see section 6.1) is measured.

The tagging efficiency ϵ is determined by counting the amount of tagged B_s^0 . Based on generator level information the original flavour content of the B_s^0 is checked and compared to the tag given by the SSKT algorithm. In this way the amount of wrong tagged B_s^0 and thus the mistag probability ω is being measured.

Due to the oscillation of the B_s^0 its flavour content at production time can be different compared to its flavour content at decay time. However according to the proper time of the B_s^0 a probability can be calculated that the B_s^0 has changed its flavour content. This is exploited to estimate ω in data and will be discussed in appendix B.

The resulting tagging performances in data and MC simulation can be seen in table 16.

Tagging Performance

	Tagging Efficiency	Mistag Probability	Tagging Power
	ϵ	ω	$\epsilon(1 - 2\omega)^2$
MC	0.126±0.003	0.273±0.010	0.026±0.002
data	0.130±0.005	0.377±0.081	0.008±0.010
data[29]	0.134±0.004	0.344±0.027	0.013±0.004

Table 16: The default tagging performance for the presented B_s^0 selection. The results are compared to a study using the same SSKT algorithm and the same SSKT cuts [29]. Like in the D_s^+ system there is a better Tagging Power in MC simulation due to a different mistag probability ω of 0.104 ± 0.082 or 0.071 ± 0.029 .

A study of the oscillation frequency has been done in [29]. As a byproduct the tagging efficiency was calculated which is quoted here. Compared to the study done in this chapter the same SSKT cuts and a similar B_s^0 selection were used. An unbinned maximum likelihood fit to the B_s^0 mass was used to determine the amount signal B_s^0 . In this way all $B_s^0 \rightarrow D_s^- \pi^+$ decay channels in which not only combinatorial background is present could be used and higher statistics could be achieved (9189 instead of 4387 PBs signal candidates).

However studying the SSKT performance it is necessary to have an unbiased look at the Tagging Track distributions and avoid systematic effects. This is achieved with using only the $B_s^0 \rightarrow D_s^- (\phi \pi^-) \pi^+$ decay channel and handle the background with sideband subtraction. Using a fit method to determine these distributions would be technically too complicated for this analysis.

There is a discrepancy in the SSKT performance in data and MC simulation. The difference in the Tagging Power is related to ω being smaller in MC simulation. The difference in ω is 0.116 ± 0.082 , i.e. looking at the result in the reference study 0.071 ± 0.029 . Both methods are consistent within statistical fluctuations and agree in the fact that the algorithm is performing better on MC simulation than in data.

In the study of the D_s^+ (see section 5) the differences in the tagging performance are similar. The default tagging efficiency is in agreement between data and MC simulation and the mistag probability is 0.062 ± 0.020 too good.

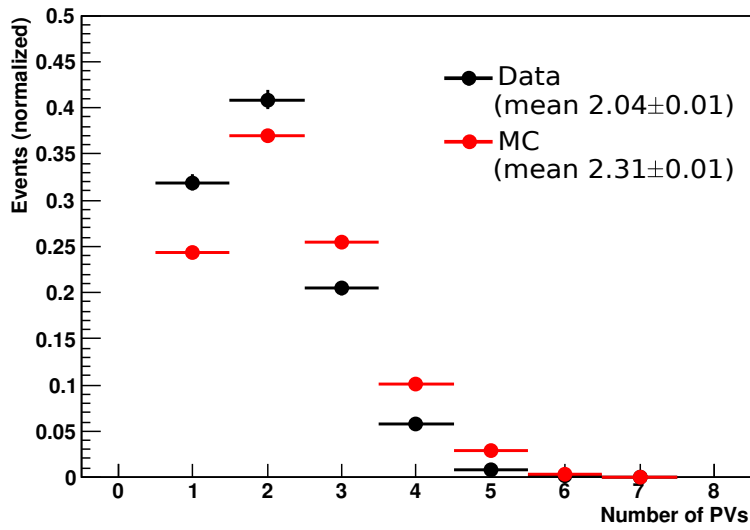


Figure 33: Number of primary vertices in the event. In MC simulation in the mean there are 0.272 ± 0.016 more PVs in the event than in data.

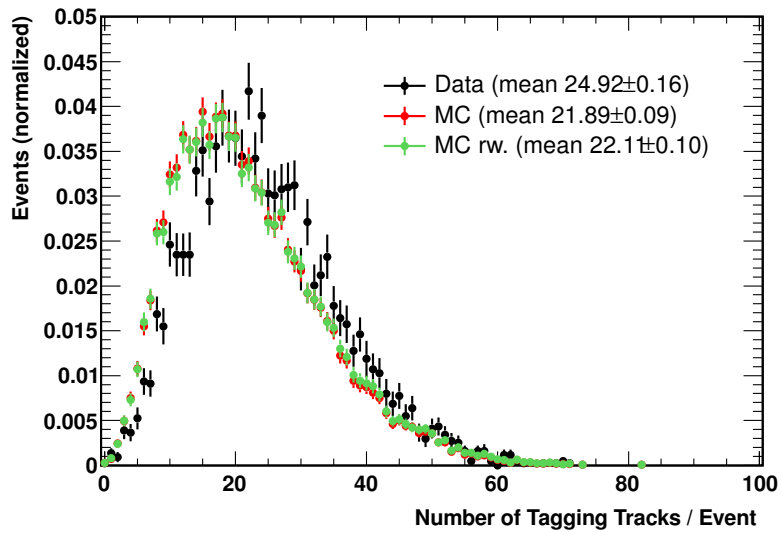


Figure 34: The Tagging Track multiplicity of data and MC simulation. Reweighting the number of PVs has no big influence on the track multiplicity. In total there are still 2.81 ± 0.19 too few tracks in the MC simulation after this correction.

6.3 Data and Simulation Comparison

6.3.1 Primary Vertex multiplicity

At first there is a check of the number of reconstructed PVs and the Tagging Track multiplicity. The PV multiplicity is too high in the MC simulation (see figure 33). In the mean there are 2.040 ± 0.013 PVs per event in data and 2.312 ± 0.009 PVs per event in MC simulation.

To correct for this difference each event from the MC simulation is reweighted according to the PV distributions. The process of reweighting is described in detail in section 5.3.2. The effect of reweighting the number of PVs on the number of Tagging Tracks distribution (see figure 34) is a change of 0.22 tracks per event. On data there are in the mean 24.92 ± 0.16 tracks whereas in the MC simulation there are without reweighting the number of PVs 21.89 ± 0.09 tracks and with doing it 22.11 ± 0.10 tracks.

The effect of reweighting is not only small on the track multiplicity but also cannot explain the large discrepancy of the mistag probability ω between data and MC simulation. The change in ω due to reweighting the number of PVs is:

$$\Delta\omega = \omega_{MC,corrected} - \omega_{MC} = -0.0026$$

Therefore the discrepancy between data and MC simulation is even larger as observed in the first place. This behavior is also seen in the D_s^+ system. The remaining difference in the track multiplicity will be discussed in section 6.3.4.

6.3.2 Track Resolution

The track resolution and thus the IPSig distribution is different in data and MC simulation (see figure 35). The same technique as described in section 5.3.3 is used to worsen(smear) the resolution in MC simulation. For Tagging Tracks the effect is overestimated and thus the mean IPSig value is in MC simulation 4.6% larger as data

In the SSKT a loose IPSig cut is used ($IPSig < 4.125$) and the majority of the tracks pass this cut. The number of tracks passing all SSKT cuts including this IPSig cut is in the *smear*d MC simulation only 1% less than for the normal MC simulation. Thus the effect on the SSKT is expected to be small.

The change in the mistag probability with this correction is:

$$\Delta\omega = \omega_{MC,smear}d - \omega_{MC} = +0.0028$$

Thus it is negligible in comparison to the discrepancy in ω of at least 0.071 ± 0.029 between data and MC simulation. The impact of this effect is of the same order than observed in the D_s^+ system ($\Delta\omega = +0.0012$).

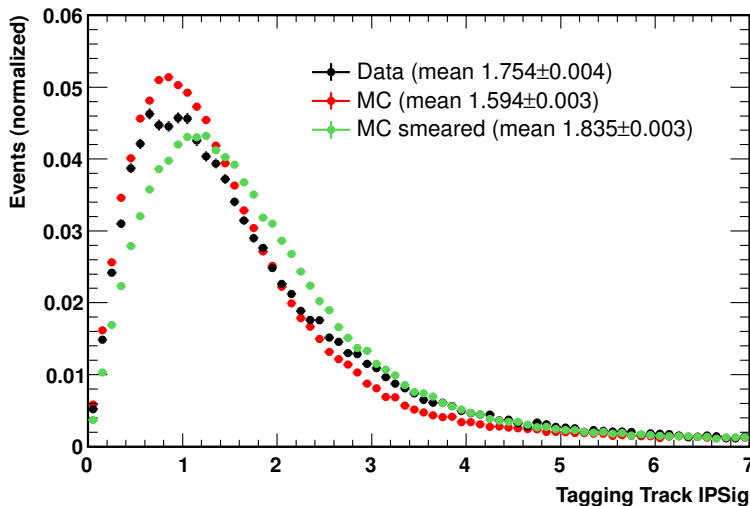


Figure 35: Tagging Track IPSig distribution for data and the MC simulation. The resolution of MC simulation is artificially worsened (smeared) to simulate the effect of a worse IPSig distribution.

6.3.3 Particle Identification

The PID performance is rather well simulated for 2010 data (see section 5.3.4). However, the RICH setup changed during data taking in the beginning of 2011. Additional CO_2 was added in the gas mixture to prevent aging due to electrical discharges. This had an effect on the refractive index of the gas and thus the size of the Cherenkov angles. As a result the PID performance changed especially for light particles such as pions. Therefore it cannot be concluded that the MC simulation which had been originally created for 2010 data also represents 2011 data.

The measurement of the PID performance was done analogously to section 5.3.4. For the B_s^0 data taken in 2011 corresponding data samples of kaons, pions and protons were provided[30]. The phase space for which this analysis could be done is limited due to statistics to:

- Kaons/Pions: P [8,50] GeV, Pt [0.8,5] GeV, η [2.5,4]
- Protons: P [8,50] GeV, Pt [0.8,5] GeV, η [2.7,4]

69% of the Tagging Tracks after all SSKT cuts are inside of this phase space. The particles from the data samples are reweighted according to properties of the Tagging Tracks from MC simulation. This is done analogously to the procedure in section 5.3.4 for quantities which are correlated to the PID performance. At first the particles are reweighted according to the number of total tracks in the event. Afterwards simultaneously the momentum and pseudorapidity of the tracks are reweighted.

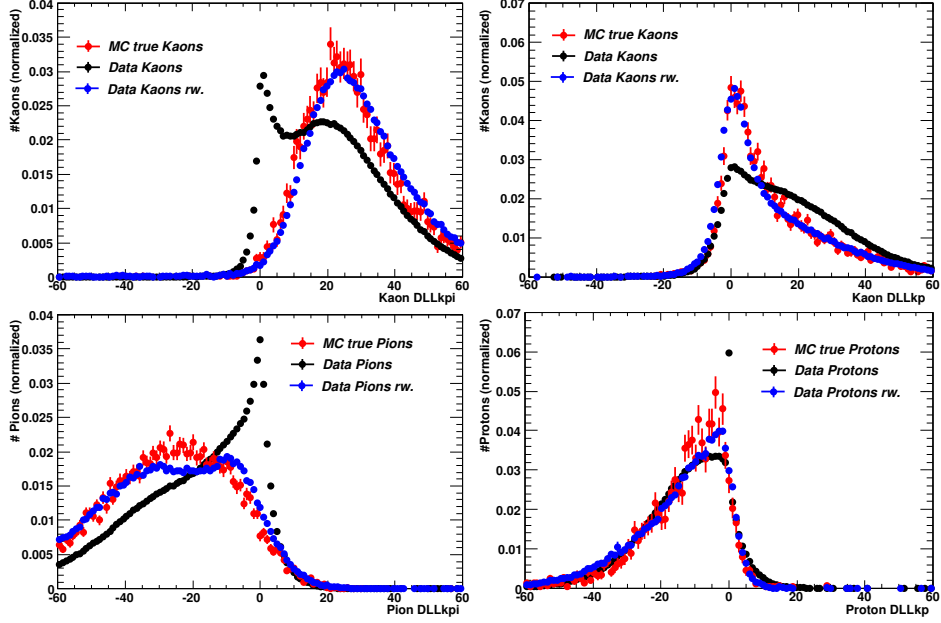


Figure 36: PID performance for kaons (top), pions (bottom left) and protons (bottom right) for data and MC simulation. Particles in data are reweighted to match the phase space of MC simulation. For the used SSKT cuts ($DLLkpi > 4.5$, $DLLkp > -8.5$) the PID performance is comparable.

The DLL distributions can be seen in figure 36. For the kaons a good agreement between data and MC simulation is present. The change in the RICH setup seems not to have a large influence in kaon PID. Regarding protons also there is agreement between data and MC simulation. In contrast a significant difference is present in the DLLkpi distribution of pions. Due to two different RICH setups two peaks are visible in the data distribution. As a result the pion separation power is overestimated in MC simulation. However, with a loose SSKT cut ($DLLkpi > 4.5$) the impact on the pion MisID probability is small.

	MC	Data reweighted
Kaon Efficiency ($DLLkpi > 4.5$)	$97.11 \pm 0.21\%$	$97.28 \pm 0.06\%$
Pion MisID Probability ($DLLkpi > 4.5$)	$3.20 \pm 0.13\%$	$3.86 \pm 0.05\%$
Kaon Efficiency ($DLLkp > -8.5$)	$98.19 \pm 0.17\%$	$97.85 \pm 0.04\%$
Proton MisID Probability ($DLLkp > -8.5$)	$41.87 \pm 0.91\%$	$40.76 \pm 0.20\%$

Table 17: Different PID performances important for the SSKT. There largest difference is 0.66 ± 0.14 percentage points in the pion MisID probability.

The corresponding PID performances of these DLL distributions can be seen in table 17. Within statistics the kaon DLLkpi efficiency as well as the proton MisID probability are in agreement. However, the PID performance of data tends to be better for these two quantities. In contrast the kaon DLLkp efficiency and the pion MisID probability are better in MC simulation. The largest difference is 0.66 ± 0.14 percentage points in the pion MisID probability. Thus the simulation of the PID is most likely not responsible for the different mistag probability of the SSKT between data and MC simulation.

This can be shown by worsening the PID performance of the MC simulation with ignoring a certain percentage of the DLL cuts as described in section 5.3.4. For a hypothetical worst case scenario the mistag probability is calculated. Using similar correction factors as for the D_s^+ analysis the effect for the present different PID performances is at least 300% overestimated. The change in ω would be:

$$\Delta\omega = \omega_{MC,worse\ PID} - \omega_{MC} = +0.010$$

Therefore the difference PID performance could not explain the different tagging performance. Comparing to the D_s^+ system the effect is of the same size ($\Delta\omega_{D_s^+,PID} < 0.0026$).

6.3.4 Underlying Event

In the D_s^+ system a major part of the different tagging performance between data and MC simulation could be explained by the Underlying Event (UE). A too low UE activity in the high momentum region important for the SSKT would have resulted in too little background. The UE activity itself does not depend directly on the signal fragmentation and therefore a similar effect can be expected for the B_s^0 .

Following the same procedure as for the D_s^+ system (see section 5.3.5) the UE can be quantified using the Tagging Track $\Delta\phi$ distribution. The UE is assumed to have in contrast to the B_s^0 fragmentation tracks a flat $\Delta\phi$ distribution. The B_s^0 fragmentation tracks itself are expected to be located at smaller $\Delta\phi$ values (see figure 13 in section 4.1). Thus above $\Delta\phi > 1$ there should be mainly tracks from the UE. Due to momentum conservation in the $b\bar{b}$ quark pair production the opposite B predominantly flies in the opposite ϕ direction¹². Therefore an increase in the number of tracks can be seen for $\Delta\phi > 2$ and this region is excluded for this analysis.

¹²This was also checked in MC simulation.

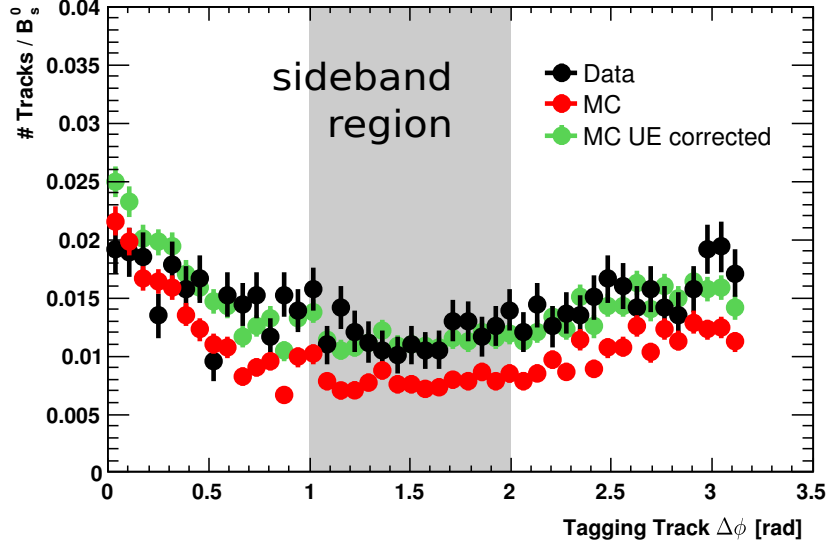


Figure 37: Tagging Track $\Delta\phi$ distribution of data and MC simulation with all SSKT cuts. In the sideband region $\Delta\phi$ [1,2] is used to quantify the UE activity. Additional background is simulated and scaled according to this region.

To estimate the effect of missing background from the UE to the tagging performance all SSKT cuts but the $\Delta\phi$ cut¹³ are applied to the Tagging Tracks. The resulting Tagging Track $\Delta\phi$ distribution can be seen in figure 37. The estimation of the UE activity is done in $\Delta\phi$ sideband region [1,2].

In this region there are $32.2 \pm 3.1\%$ too few tracks in MC simulation.

It can be assumed that the same amount of UE tracks is missing also in the $\Delta\phi$ region used by the SSKT. The effect on the tagging performance if this missing tracks from the UE would be artificially added will be estimated. In a first step a theoretical analysis is done and afterwards the missing background is simulated. For the measurement of the mistag probability the $\Delta\phi$ cut will be applied again.

Theoretical change in $\Delta\omega$ due to the UE

To estimate the effect of additional background in MC simulation equation 1 derived in section 5.3.5 is used. It is based on the fact that most of the particles (for the B_s^0 87%) are untagged. Thus in a good approximation an additional Tagging Track passing all SSKT cuts results in an additional random tagged B_s^0 . Having a random tag this has to be added to the total number of all tagged B_s^0 and in 50% of the cases to the number of wrong tagged B_s^0 .

¹³and also not ΔQ which is correlated to $\Delta\phi$ (see section 5.3.5).

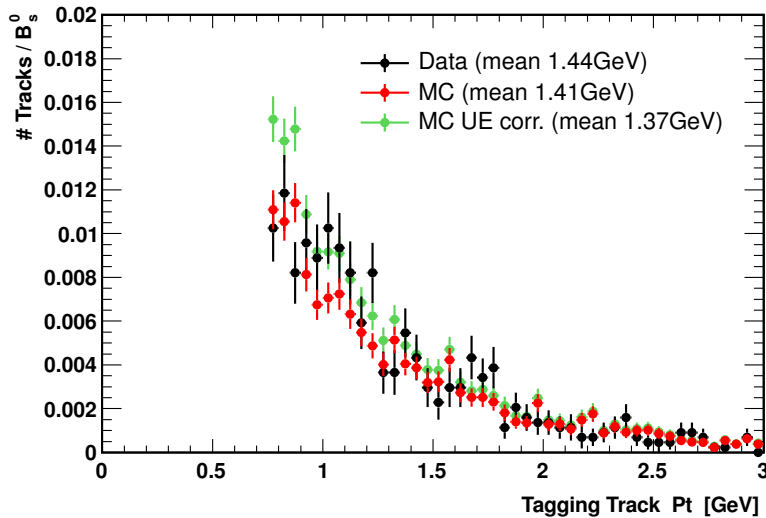


Figure 38: Tagging Track transverse momentum distribution. The plots are scaled to the number of B_s^0 . Additional background has on average a smaller transverse momentum than the other tracks.

Two systematic uncertainties are considered. Omitting the ΔQ cut changes the mistag probability in MC simulation $\Delta\omega = -0.00067$. The absolute value of this number is taken as uncertainty for ω . Additionally the maximal possible influence of the 13% tagged B_s^0 is calculated. The two extrema would be if for these B_s^0 additional Tagging Tracks would be either ignored or would replace a right tag.

Using the formula on the present values results in:

$$\Delta\omega_{theo} = \omega_{MC+32\%moreUE} - \omega_{MC} = +0.0469 \pm 0.0063 \text{ (stat.) } \begin{matrix} +0.0015 \\ -0.0055 \end{matrix} \text{ (syst.)}$$

This is again a large effect which would explain a large part of the discrepancy in the mistag probability between data and MC simulation. However, similar to the D_s^+ system, this $\Delta\omega$ is too small to be able to explain the total difference observed.

Simulating missing UE with minimum bias data

The simulation of additional UE is done similar as outlined in section 5.3.5. Tracks from an independent MC10 minimum bias data sample are used as additional Tagging Tracks. The amount of additional tracks is scaled in a way that there is agreement in the $\Delta\phi$ middle region $\Delta\phi$ 1-2 after the SSKT cuts, but the ΔQ cut (see figure 37). The Tagging Track transverse momentum spectrum can be seen in figure 38. The additional background has on average a smaller transverse momentum than the already present tracks in data. This would be explained by the assumption that the UE in data has compared to MC simulation on average a higher momentum and

Tagging Efficiency ϵ	
Data	0.1381 ± 0.0055
MC simulation	0.1328 ± 0.0029
MC simulation with additional UE	0.1612 ± 0.0031

Table 18: Tagging efficiency ϵ of data and MC simulation without ΔQ cut. With simulating additional UE ϵ is increased in MC simulation and it is no longer in agreement with data.

thus there is a higher amount of them in the high Pt region. The next step would be to reweight the underlying event of MC simulation according to data what is however not done in this diploma thesis.

For the uncertainty of this correction the amount of additional background is varied by $\pm 10\%$. Because the additional background is scaled to data after the SSKT cuts the different Pt distributions of data and MC simulation are negligible concerning the effect on the tagging performance. The measured effect on the mistag probability is in agreement with the theoretical expectation:

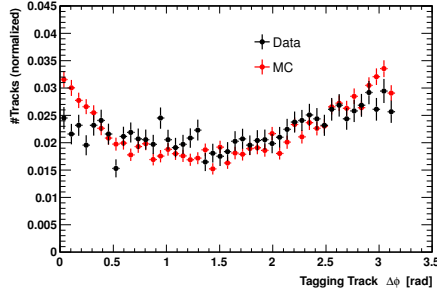
$$\Delta\omega_{sim} = \omega_{MC, no DQ cut + minBias} - \omega_{MC, no DQ cut} = +0.0427_{-0.003}^{+0.004}$$

The tagging efficiency ϵ of the MC simulation is with this correction no longer in agreement with data. It is increased by 0.029 and is thus too large (see table 18). It is therefore likely that, as in the D_s^+ system, there is a further discrepancy between data and MC simulation.

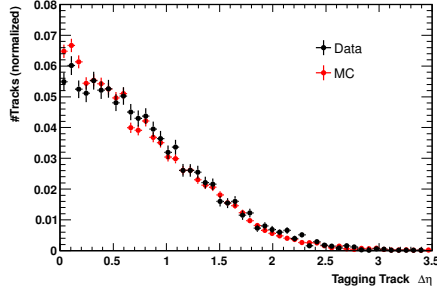
6.3.5 Fragmentation

The fragmentation of B_s^0 mesons is different from D_s^+ mesons. Furthermore the phenomenological model used in Pythia to simulate these fragmentations describes the B_s^0 system more accurate than the D_s^+ (see section 3.2.2). Therefore even if the D_s^+ fragmentation (see section 5.3.6) would be described incorrectly this does not have to be true for the B_s^0 fragmentation. The observed effect in the D_s^+ system is that there are too many fragmentation tracks simulated in the high Pt region. This also would result in a too high tagging efficiency ϵ in the MC simulation after the UE correction. As seen in the last section ϵ is also too high in the B_s^0 system after the UE correction.

Tagging Track $\Delta\phi$



Tagging Track $\Delta\eta$



Tagging Track ΔQ

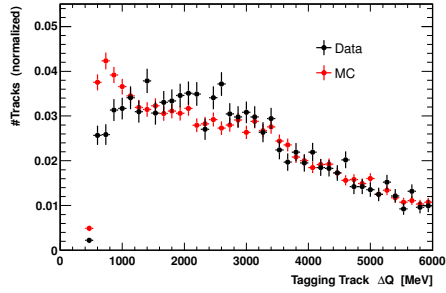


Figure 39: Tagging Track $\Delta\phi$, $\Delta\eta$ and ΔQ distributions. Additional cuts applied are $P_t > 900$ MeV, $IP_{Sig} > 5$ and $DLL_{kpi} > 5$. In all plots for smaller values there is a discrepancy between data and the MC simulation. These are the regions where also the B_s^0 fragmentation tracks are supposed to be.

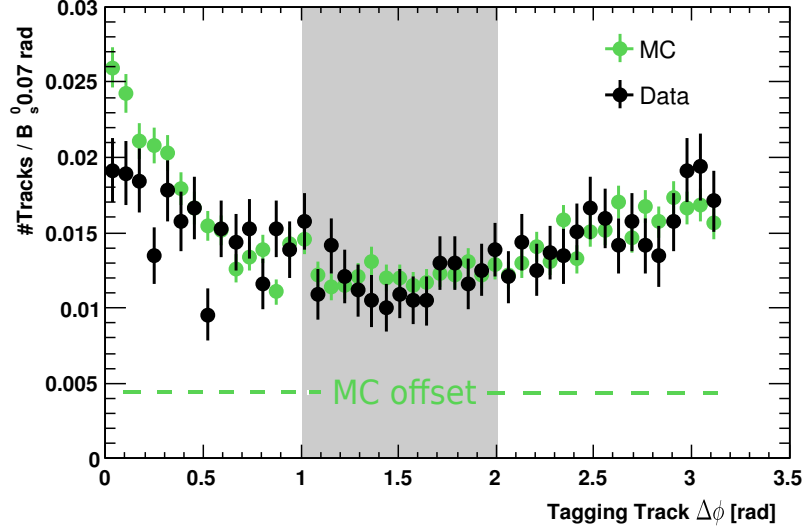


Figure 40: Tagging Track $\Delta\phi$ distribution for data and MC simulation with an offset to compensate for missing UE. The offset is scaled to data in the region $\Delta\phi$ [1,2]. The remaining difference for $\Delta\phi < 0.7$ is assumed to be related to a different amount of fragmentation tracks.

A possibility to visualize the B_s^0 fragmentation tracks are the Tagging Track $\Delta\phi$, $\Delta\eta$ and ΔQ distributions as seen in figure 39.

To enhance the ratio of B_s^0 fragmentation tracks compared to all tracks additional cuts are applied to the Tagging Track selection. To allow a better comparison to the D_s^+ system the same cuts are used as in figure 28. As the momentum is assumed to be simulated well a hard momentum cut ($P_t > 900$ MeV) is used. Also an IPSig cut ($\text{IPSig} < 5$) and PID cut ($\text{DL-Lkpi} > 5$) are applied, because these variables are tested in section 6.3.2 and section 6.3.3.

Similar to the D_s^+ system the MC simulation is differing from data in the regions where the fragmentation tracks are supposed to be located. These are the regions $\Delta\phi < 0.5$, $\Delta\eta < 0.5$ and $\Delta Q < 1500$ MeV. There are too many tracks in MC simulation in these regions.

A rough estimation of the impact of a different fragmentation is done in the following way. In the Tagging Track $\Delta\phi$ distribution in MC simulation a flat offset is added (see figure 40). This is done to simulate the missing UE. In the region $\Delta\phi$ [1,2] the offset is scaled so that there are the same number of tracks in data and MC simulation. Compared to the simulation of additional UE with minimum bias tracks done in the last subsection the same result is received but without statistical fluctuations.

It is assumed that after this UE correction the remaining difference is due to a different amount of B_s^0 fragmentation tracks. After all SSKT cuts but the ΔQ cut there are in the mean 0.155 ± 0.006 tracks in data and 0.183 ± 0.007

tracks in the corrected MC simulation. Thus there would be 0.028 ± 0.009 ($15.3 \pm 4.6\%$) too many fragmentation tracks in the MC simulation.

Only 9.2% of the tagged B_s^0 has more than one Tagging Track passing all SSKT cuts. Thus in a good approximation equation 2 derived in section 5.3.6 can be used to estimate the change in the mistag probability ω . In this formula it is assumed that the removal of a Tagging Track is equal to the removal of the tag of the corresponding B_s^0 . Therefore by removing a B_s^0 fragmentation track the number of all tagged B_s^0 is reduced by one whereas the number of wrong tagged B_s^0 stays the same. For the presented values with $y = \#(\text{too many frag tracks})/\#(\text{all tracks}) = 0.028/0.183$ this would result in:

$$\Delta\omega(y = 0.153) = \omega_{MC-Frag} - \omega_{MC} = 0.057 \pm 0.020 \text{ (stat.)}$$

Due to adjusting the Tagging Track multiplicity in MC simulation to data also the tagging efficiency ϵ is equalized in both samples.

Therefore like in the D_s^+ system an incorrect description of the B_s^0 fragmentation would explain a large part of the different mistag probability between data and the MC simulation. Together with a higher UE activity these corrections could explain the total observed discrepancy of the tagging performance between data and MC simulation. Both the tagging efficiency and the mistag probability would be within statistical uncertainties in agreement.

6.4 Summary

The same corrections as in the D_s^+ system are tested and applied. Their effects on the tagging performance can be seen in table 19. The detector is within statistical uncertainties well described in the MC simulation. The possible effects of a different track reconstruction or PID performance are small. Compared to the total different mistag probability ω between data and MC simulation these effects are too small to be a possible explanation for the observed discrepancy.

Like in the D_s^+ system it is shown that an incorrect description of the underlying event and the B_s^0 fragmentation can be reasons for the different tagging performance.

MC simulation is corrected for $32.2 \pm 3.1\%$ missing underlying event activity. After this there are in the phase space region used by the SSKT $15.3 \pm 4.6\%$ too many tracks in MC simulation which are assumed to come from the B_s^0 fragmentation. Correcting both effects would result in an unchanged tagging efficiency but a significant larger mistag probability explaining the observed difference in the tagging performance between data and MC simulation.

MC Correction	Effect on ω
primary vertex multiplicity	- 0.003
track impact parameter	< +0.003
PID performance	< +0.010
underlying event	$+0.047 \pm 0.006$ (stat.) $^{+0.002}_{-0.006}$ (syst.)
B_s^0 fragmentation	$\approx + 0.057 \pm 0.020$ (stat.)
in total	+ 0.101
Observed Difference	
Data - MC	$+ 0.104 \pm 0.082$
Data from [28] - MC	$+ 0.071 \pm 0.029$

Table 19: Effects on the mistag probability ω for different corrections done in MC simulation. The observed difference can be explained.

7 Summary and Conclusion

The determination of the production flavour of B hadrons is a crucial ingredient to many of the key analyses of LHCb. Based on experience from previous experiments e.g. CDF [22] and on LHCb simulation, the SSKT algorithm has the potential to contribute to the overall tagging performance by a factor of 1.5. However first studies on data indicate a worse performance. This thesis is dedicated to a detailed investigation of various effects which potentially cause this difference. Two systems are studied the D_s^+ and the B_s^0 . While the B_s^0 and D_s^+ fragmentation are expected to be different this is not the case for detector effects and the underlying event which therefore can also be studied in the D_s^+ system for which high statistics is available. In the first part of this thesis the Same Side Kaon Tagger (SSKT) performance was studied using $D_s^+ \rightarrow \phi \pi^+$ decays reconstructed in 36 pb^{-1} of data from 2010. As well in this mode the tagging performance in MC simulation was observed to be significant better than in data. Multiple properties related to tagging like the PID efficiency and detector resolution were compared in data and MC simulation and if necessary corrected for in MC simulation. The largest impacts on the tagging performance have equally a correction of the multiplicity of tracks from the underlying event and a correction of the D_s^+ fragmentation properties. Both effects together can explain the observed discrepancy in tagging performance between data and MC simulation.

In the second part the SSKT performance was tested on $B_s^0 \rightarrow D_s^- (\phi \pi^-) \pi^+$ decays in 341 pb^{-1} data recorded in 2011. Like in the D_s^+ system the SSKT was performing in MC simulation significantly better than in data. A similar study like for the D_s^+ decay was performed. As well the largest impact has the correction of the track multiplicity of the underlying event. Due to the fast mixing of the B_s^0 and low statistics it was not possible to study the fragmentation like in the D_s^+ system. However remaining differences between data and MC simulation after the corrections indicate that the B_s^0 fragmentation is described incorrectly. With the correction of the underlying event multiplicity and the assumption of a incorrect described B_s^0 fragmentation the observed discrepancy in the tagging performance between data and MC simulation can be explained.

In both systems in MC simulation there are too many tracks from the D_s^+/B_s^0 fragmentation in the high momentum region used by the SSKT. A possible explanation for the excess of tracks from the D_s^+/B_s^0 fragmentation would be a too soft fragmentation function in the event generation. In that case other particles from the fragmentation but the D_s^+/B_s^0 would have a higher momentum and there would be a higher amount of them in the high momentum region. The next step will be to further investigate this fragmentation process in MC simulation.

A Optimizing D_s^+ Same Side Kaon Tagger

Detailed information about the SSKT algorithm is given in section 4.1. In the following it is explained how the SSKT algorithm is tuned by changing the SSKT cuts to maximize the tagging performance. The procedure starts with a certain set of SSKT cuts. One cut is chosen and varied whereas the other ones are locked. Changing a cut also changes the mistag probability and the tagging efficiency. By making the cut looser the tagging efficiency gets higher and the mistag probability gets worse. The optimal cut value is at the point of the largest tagging power. The value of the cut under investigation is set to this value.

Afterwards this cut is locked and another cut is chosen to be investigated and changed to the optimal cut value. In this way consecutively all cuts are adjusted.

Optimal Cut values	
P >	4000 MeV
Pt >	850 MeV
IPSig <	5
Track χ^2 /ndf <	5
$\Delta\eta$ <	0.8
$\Delta\phi$ <	0.9
ΔQ <	1600
DLLkpi >	5
DLLkp >	-5

Table 20: The optimized SSKT cuts for MC simulation.

Because of correlations between the cuts the whole procedure is done several times until the preferred cut variables stay stable.

As an example the dependency of the tagging power on the cut on the Tagging Track transverse momentum is shown in figure 41. What can be seen is that above a Pt cut of 850 MeV the Tagging Power stays within fluctuations unchanged. In this cases a conservative cut at 850 MeV is chosen to not optimize on fluctuations and enlarge statistics.

To avoid the procedure to converge into local minima the whole procedure is done multiple times with choosing each time different starting values.

The optimal cut values for MC simulation are listed in table 20.

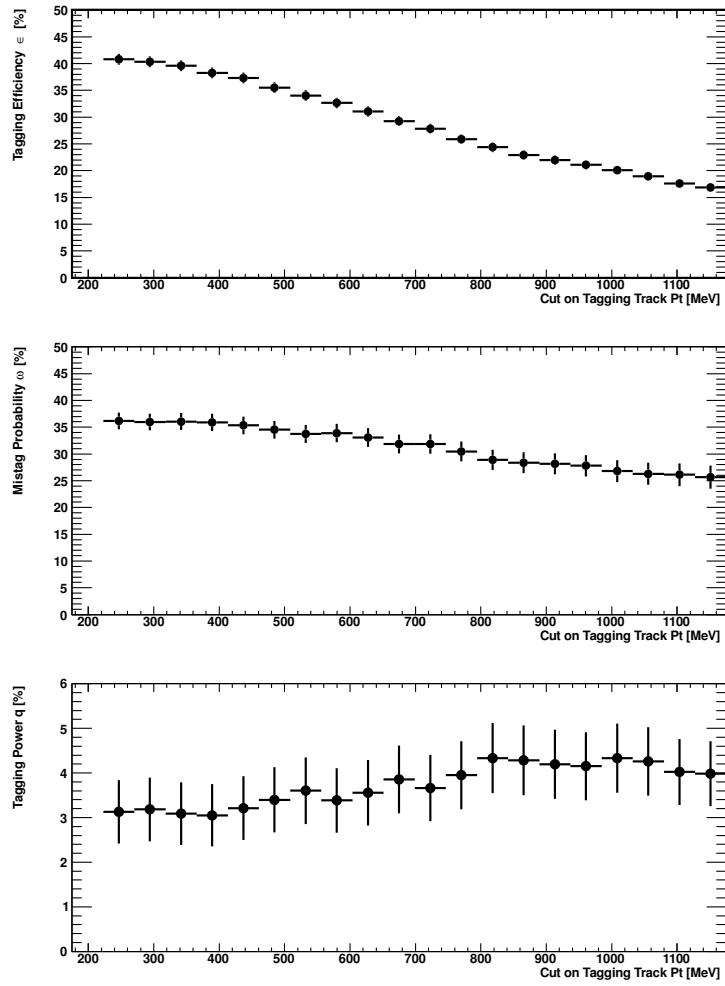


Figure 41: The SSKT tagging performance for the MC optimized SSKT cuts but different cuts on Pt. It is shown the tagging efficiency ϵ (top), the mistag probability ω (middle) and the tagging power q (bottom). Error bars indicate the statistical uncertainty of the value and are correlated for different cuts.

B Estimating the mistag probability for the mixing B_s^0 meson

The challenge in the B_s^0 system is to determine the mistag probability of the SSKT algorithm. As the B_s^0 is oscillating its flavour content is changing over time. Thus in contrast to the D_s^+ system the knowledge about the flavour content at decay time does not provide the direct possibility to check the tagging decision given by the SSKT.

In MC simulation the tag is compared to the B_s^0 original flavour content taken from generator level information. In data information is received using the correlation from the mixing probability to the decay time. The mixing can be described in an approximation by a cosine and thus the number of mixed B_s^0 $n_{mix}(t)$ compared to all B_s^0 in the event $n(t)$ can be written as

$$n_{mix}(t) = n(t) (0.5 - 0.5 \cdot \cos(\Delta m_s \cdot t))$$

For oscillation studies it is useful to look at the mixing Asymmetry $A(t)$:

$$A(t) = \frac{n_{unmix}(t) - n_{mix}(t)}{n_{unmix}(t) + n_{mix}(t)} = \cos(\Delta m_s \cdot t)$$

The factor $n(t)$ is canceling and thus theoretically a cosine with the amplitude 1 should be observable. The frequency of this oscillation is still Δm_s and in this way the B_s^0 mixing frequency can be obtained.

For the estimation of ω the fact can be used that not a amplitude equal to one but a smaller one measured. The measured amplitude is reduced by mainly two effects. On the one hand the flavour taggers identify a fraction of ω of the B_s^0 candidates wrong. This dilution results in a reduction of the amplitude by the factor $(1 - 2\omega)$. On the other hand the time resolution of the detector is limited. This affects the amplitude as $\exp(-\frac{1}{2}\sigma_{ct}^2 \Delta m_s^2)$, where σ_{ct} is the proper time resolution. Both effects together result in

$$A = (1 - 2\omega) \exp(-\frac{1}{2}\sigma_{ct}^2 \Delta m_s^2)$$

Therefore with knowledge about the mixing frequency and the proper time resolution of the detector measuring the amplitude of the mixing asymmetry the mistag probability can be estimated:

$$\omega = \frac{1 - A \cdot \exp(+\frac{1}{2}\sigma_{ct}^2 \Delta m_s^2)}{2}$$

The mixing amplitude of data for default SSKT cuts can be seen in figure 42. The mixing frequency Δm_s was measured independently to be $\Delta m_s = 17.63 \text{ ps}^{-1}$ [26]. In an analysis using similar data the proper time resolution was determined to be about 45 fs [28].

Therefore with measuring an amplitude of the mixing asymmetry $A = 0.180 \pm 0.059$ the mistag probability can be estimated to be $\omega = 0.377 \pm 0.081$. To cross check this method, ω is also calculated in this way for MC simulation. The proper time resolution in MC simulation was determined to be $\sigma_{ct,MC} = 40.3$ fs using generator level information. The mixing amplitude in MC simulation for default SSKT cuts is shown in figure 43. The mistag probability obtained using this method ($\omega = 0.271 \pm 0.041$) is comparable to the one measured by using directly generator level information ($\omega = 0.270 \pm 0.010$).

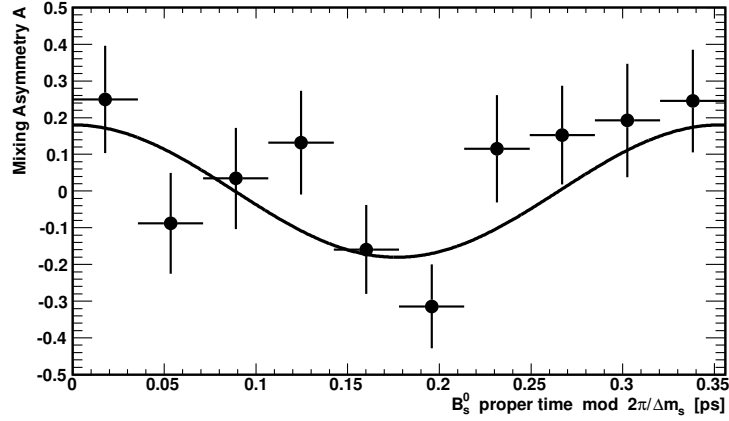


Figure 42: Mixing amplitude of data using the default B_s^0 SSKT cuts. The size of the amplitude is related to the mistag probability. In this case the amplitude of the mixing asymmetry $A = 0.180 \pm 0.059$ concludes $\omega = 0.377 \pm 0.081$.

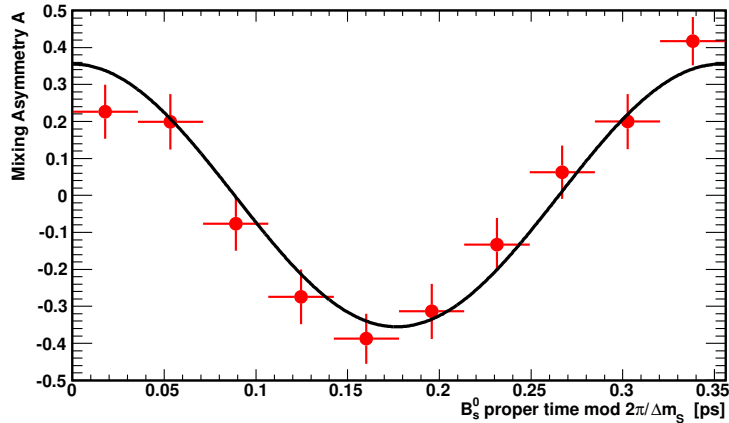


Figure 43: Mixing amplitude of MC simulation and default B_s^0 SSKT cuts. With the amplitude of the mixing asymmetry $A = 0.355 \pm 0.032$ the mistag probability is estimated to be $\omega = 0.271 \pm 0.041$ what is compatible to the one obtained using MC generator level information which is $\omega = 0.270 \pm 0.010$.

References

- [1] C. S. Wu, E. Ambler, R. W. Hayward, D. D. Hoppes, R. P. Hudson: Experimental Test of Parity Conservation in Beta Decay. In: Physical Review. 105, 1957, S. 1413-1415. doi:10.1103/PhysRev.105.1413
- [2] J. Christenson, J. Cronin, V. Fitch and R. Turlay, Phys. Rev. Lett. 13, 138 (1964); J. M. Gaillard et al., ibid, 18, 20 (1967); J. Cronin et al. ibid, 18, 25 (1967)
- [3] The Large Hadron Collider LHC (<http://lhc.web.cern.ch/lhc/>)
- [4] Tevatron particle accelerator (<http://www-bdnew.fnal.gov/tevatron/>)
- [5] CERN - the European Organization for Nuclear Research (<http://public.web.cern.ch/public/>)
- [6] The LHCb Collaboration, The LHCb Detector at the LHC, JINST 3, S08001 (2008)
- [7] LHC Welt Maschine (http://www.weltmaschine.de/cern_und_lhc/lhc/)
- [8] LHCb physics prospects for CP violation measurements with 1 fb^{-1} - Poluektov, A - LHCb-PROC-2010-045
- [9] The LHCb Collaboration, Roadmap for selected key measurements of LHCb (2009)
- [10] The GAUSS Project (<http://lhcb-release-area.web.cern.ch/LHCb-release-area/DOC/gauss/>)
- [11] Pythia (<http://home.thep.lu.se/~torbjorn/Pythia.html>)
- [12] EvtGen package (<http://www.slac.stanford.edu/~lange/EvtGen/>)
- [13] The BOOLE Project (<http://lhcb-release-area.web.cern.ch/LHCb-release-area/DOC/boole/>)
- [14] T. Sjostrand, S.Mrenna, P. Skands, Pythia 6.4 Physics and Manual, JHEP 05 (2006) 026 (LU TP 06-13, FERMILAB-PUB-06-052-CD-T, hep-ph/0603175)
- [15] T. Sjostrand, Monte Carlo generators for the LHC, Academic Training Lecture
- [16] B. Povh, Teilchen und Kerne: Eine Einführung in die physikalischen Konzepte (ISBN-10: 3540210652)

- [17] C. Peterson, D. Schlatter, I. Schmitt and P. Zerwas, Phys. Rev. D27 (1983) 105
- [18] P. Z. Skands, Tuning Monte Carlo Generators: The Perugia Tunes, arXiv:1005.3457v4 [hep-ph]
- [19] K. Nakamura et al. (Particle Data Group), J. Phys. G 37, 075021 (2010) and 2011 partial update for the 2012 edition.
- [20] H.-G Moser, A Roussarie, Mathematical methods for $B^0\bar{B}^0$ oscillation analyses, Nuclear Instruments and Methods in Physics Research Section A: Accelerators, Spectrometers, Detectors and Associated Equipment, Volume 384, Issues 2-3, 1 January 1997, Pages 491-505
- [21] Babar, A measurement of the $B^0\bar{B}^0$ oscillation frequency and determination of flavor-tagging efficiency using semileptonic and hadronic B^0 decays, SLAC-PUB-8530 (2000)
- [22] CDF collaboration, Observation of $B_s - \bar{B}_s$ Oscillation, Phys.Rev.Lett.97:242003,2006
- [23] The LHCb Collaboration, LHCb Flavour Tagging Performance, CERN-LHCb-2003-115
- [24] The LHCb Collaboration, Flavour Tagging Algorithms and Performances in LHCb, CERN-LHCb-2007-058
- [25] The LHCb Collaboration, Optimization and calibration of the LHCb flavour tagging performance using 2010 data, LHCb-ANA-2011-003
- [26] The LHCb Collaboration, Measurement of Δm_s in the decay $B_s \rightarrow D_s(K^+K^-\pi^-)\pi^+$ and $B_s \rightarrow D_s(K^+K^-\pi^-)\pi^+\pi^+\pi^-$, LHCb-ANA-2011-005
- [27] The LHCb Collaboration, Measurement of Δm_d in $B^0 \rightarrow D^-(K^+\pi^-\pi^-)\pi^+$, LHCb-ANA-2011-015
- [28] in The LHCb Collaboration, Measurement of Δm_s in the decay $B_s \rightarrow D_s(K^+K^-\pi^-)\pi^+$ and measurement of the Same Side kaon tagging performance, LHCb-ANA-2011-043-v3
- [29] The LHCb Collaboration, Measurement of Δm_s in the decay $B_s \rightarrow D_s(K^+K^-\pi^-)\pi^+$ using opposite-side and same-side tagging algorithms, LHCb-CONF-2011-050-v2
- [30] A. Powell, Oxford University (a.powell1@physics.ox.ac.uk)
- [31] M. Pivk, sPlot: a statistical tool to unfold data distributions (2005), arXiv:physics/0402083v3